Quantized Event-Driven Simulation for Integrated Energy Systems with Hybrid Continuous-Discrete Dynamics

Peng Li[a], Shuang Li[a], Hao Yu[a]*, Jinyue Yan[b], Haoran Ji[a], Jianzhong Wu[c], Chengshan Wang[a]

[a] Key Laboratory of Smart Grid of Ministry of Education, Tianjin University, Tianjin 300072, China

[b] School of Business, Society and Engineering, Mälardalen University, Västerås 72123, Sweden

[c] Institute of Energy, School of Engineering, Cardiff University, Cardiff CF24 3AA, UK

Abstract: Effective simulation methods are becoming critically essential for the analysis of integrated energy systems (IESs) to reveal the interactions of multiple energy carriers. The incorporation of various energy technologies and numerous controllers make the IES a heterogeneous system, which poses new challenges to simulation methods. This paper focuses on the simulation of an IES with hybrid continuous-discrete properties and heterogeneous characteristics. First, a modified third-order quantized state system (MQSS3) method is proposed for the simulation of district heating systems (DHSs), in which quantized state system (QSS) and time-discretized integration are integrated to efficiently manage numerous discrete control actions. Second, an event-driven framework is established to integrate MQSS3 into the simulation of the electricity-heat integrated energy system (EH-IES). This framework enables the adoption of the most suitable models and algorithms for different systems to accommodate the heterogeneous properties of an IES. Case studies of an EH-IES with maximum 80% PV penetration and 210 buildings demonstrate that the dynamic interactions between the DHS and the power distribution network are accurately illustrated by the proposed simulation methods, in which MQSS3 indicates the highest simulation efficiency. It is also demonstrated in the simulation results that

* Corresponding author.
E-mail address: tjuyh@tju.edu.cn.

the flexibility from DHS can be utilized as demand-side resource to support the operation of power distribution network in aspects such as consuming the surplus PV generations.

Key words: dynamic simulation; integrated energy system (IES); continuous-discrete hybrid system; quantized state system (QSS); event-driven

Nomenclature

Abbreviations

EB	Electric boiler
DG	Distributed generation
HTF	Heat transfer fluid
EH-IES	Electricity-heat integrated energy system
EPS	Electric power system
DHS	District heating system
NGS	Natural gas system
IEEE	Institute of Electrical and Electronics Engineers

Sets

Ω_{c}	Set of controlled variables
Ω_{s}	Set of control states of the EBs
Ω_{v}	Set of voltages of the electricity nodes connected to the EBs

Indices

α	Indices of the pipelines, from 1 to N_{p}
β	Indices of the EBs, from 1 to N_{s}
γ	Indices of the buildings and fan coil units, from 1 to N_{b}
i, j	Indices of the state and quantized variables in the DHS, from 1 to N_{q}

$\boldsymbol{x}_{\mathrm{d}}^{(1)}$,$\boldsymbol{x}_{\mathrm{d}}^{(2)}$,$\boldsymbol{x}_{\mathrm{d}}^{(3)}$, $\boldsymbol{x}_{\mathrm{d}}^{(i)}$	First, second, third and ith-order derivatives of the state variables $\boldsymbol{x}_{\mathrm{d}}$
$\boldsymbol{q}_{\mathrm{d}}^{(1)}$, $\boldsymbol{q}_{\mathrm{d}}^{(2)}$	First and second-order derivatives of the quantized state variables $\boldsymbol{q}_{\mathrm{d}}$
$x_{\mathrm{d,max}}^{(3)}$	The element with the largest absolute value in vector $\boldsymbol{x}_{\mathrm{d}}^{(3)}$
$\boldsymbol{u}_{\mathrm{e}}^{\mathrm{c}}, \boldsymbol{u}_{\mathrm{d}}^{\mathrm{c}}$	Coupling variables of the EPS and DHS
$\boldsymbol{u}_{\mathrm{d}}, \boldsymbol{u}_{\mathrm{d}}^{-}$	Next control states and previous control states
$\boldsymbol{x}, \boldsymbol{q}$	State variables and quantized variables
$t_i^{\mathrm{L}}, t_i^{\mathrm{N}}$	Last and next update times of quantized variable i (s)
ΔQ	Value of the quantum
$t_{\mathrm{d}}, h_{\mathrm{d}}$	Current update time and step size for the next internal update step in the DHS (s)
t_i^{state}, t	Occurrence time of the state event of state variable i and current simulation time (s)
$t_{\mathrm{e}}, h_{\mathrm{e}}$	Current update time and step size for the next internal update step in the EPS (s)
$\boldsymbol{Y}, \boldsymbol{U}, \boldsymbol{I}$	Admittance matrix, bus voltages and injection currents of power networks
$\widetilde{\boldsymbol{x}}_{\mathrm{d}}$	Exact solutions of the state variables
$\boldsymbol{\varepsilon}_{\mathrm{LTE}}, \boldsymbol{e}(t)$	Local truncation error and global error
$u'_{\mathrm{d},k}$, $u''_{\mathrm{d},k}$	The current value of discrete variable k and the value of discrete variable k when event B was last triggered
$y'_{\mathrm{e},k}$, $y''_{\mathrm{e},k}$	The value of algebraic variable k at the current time and the value of algebraic variable k when event A was last triggered

Parameters

N_{p},N_{s},N_{b},N_{q}	Total number of pipelines, EBs, buildings and state variables

Variables		N_α	The number of control volumes of pipeline α
T_α^{p}	Temperature of the HTF in pipeline α (℃)	$\rho_{\mathrm{p}}, c_{\mathrm{p}}, \lambda$	Density (kg/m^3), specific heat capacity (J/(kg·℃) and thermal conductivity (W/(℃·m)) of the HTF
$T_{\alpha,n}^{\mathrm{p}}$	Temperature of control volume n of pipeline α (℃)	$A_\alpha^{\mathrm{p}}, R_\alpha^{\mathrm{p}}, \Delta x, D_\alpha^{\mathrm{p}}$	Cross-section area (m^2), thermal resistance ((℃·m)/W), spatial step (m) and diameter (m) of pipeline α
T_α^{n}	The temperature of the node connected to the inlet of pipeline α (℃)	$m_\beta^{\mathrm{s}}, m_\gamma^{\mathrm{f}}$	Mass of the HTF in EB β and fan coil unit γ (kg)
T^{a}	Ambient temperature (℃)	R^{s}	Resistance of a heating unit (Ω)
$T_\beta^{\mathrm{s,in}}, T_\beta^{\mathrm{s,out}}$	Inlet and outlet temperatures of EB β (℃)	$T_\beta^{\mathrm{s,max}}, T_\beta^{\mathrm{s,min}}$	Upper and lower limits of the outlet temperature of EB β (℃)
U_β^{s}	Voltage of the electricity node connected to EB β (V)	$K_\gamma^{\mathrm{f}}, A_\gamma^{\mathrm{f}}$	Heat transfer coefficient (W/(m^2·℃)) and radiating area (m^2) of fan coil unit γ
N_β^{s}	Number of active heating units in EB β	$g_\alpha^{\mathrm{p}}, g_\beta^{\mathrm{s}}, g_\gamma^{\mathrm{f}}$	Mass flow rates through pipeline α, EB β and fan coil unit γ (kg/s)
$T_\gamma^{\mathrm{f,in}}, T_\gamma^{\mathrm{f,out}}$	Supply and return temperatures of fan coil unit γ (℃)	$\rho_{\mathrm{a}}, c_{\mathrm{a}}$	Density (kg/m^3) and specific heat capacity (J/(kg·℃)) of indoor air
T_γ^{b}	Indoor temperature of building γ (℃)	$K_\gamma^{\mathrm{b}}, V_\gamma^{\mathrm{b}}$	Volumetric heat index (W/(m^3·℃)) and peripheral volume (m^3) of building γ
$Q_\beta^{\mathrm{s}}, Q_\gamma^{\mathrm{f}}$	Heat power produced by EB β and fan coil unit γ (W)	$T_\gamma^{\mathrm{b,max}}, T_\gamma^{\mathrm{b,min}}$	Upper and lower limits of the indoor temperature of building γ (℃)
S_γ^{f}	Bool variable indicating the switch status of fan coil unit γ	$L^{\max}, L^{\min}$	Upper and lower limits of the controlled state variables (℃)
$\boldsymbol{x}_{\mathrm{e}}, \boldsymbol{y}_{\mathrm{e}}$	State variables and algebraic variables of the EPS	t_0, t_{end}	Initial and end times of the simulation (s)
$\boldsymbol{x}_{\mathrm{d}}, \boldsymbol{q}_{\mathrm{d}}$	State variables and quantized variables of the DHS	Δy_{e}	Impact threshold (V)

1. Introduction

With increasing concern on energy sustainability, conventional individual energy systems are evolving toward integrated energy systems (IESs), which are a promising paradigm for provid-

ing economic and environmental benefits by coordinating multiple energy carriers [1]. Consequently, IESs have become increasingly complex with the incorporation of different energy technologies such as various energy sources, networks, demands, and energy conversion devices. These complexities pose new challenges for IESs in terms of the system operation [2], design [3][4], analysis [5] and control [6]. Particularly, driven by the electrification of end-user energy consumption, electric networks are more closely coupled with other types of energy demands, such as heat, in communities and urban areas [7]. In this condition, district heating systems (DHSs) for residential heating become an impactive load of electric power systems (EPSs), introducing various influencing factors such as ambient temperature, building parameters, and user behaviors into the EPS. These factors make the loads from heat demand significantly different from the regular electric loads and are generally treated as uncertainties in the operation of EPSs [8]. Meanwhile, inertia of heat networks and demand response of heat users can provide flexibility to the EPSs [9].

In the energy sector, simulation methods have been extensively studied and developed for individual energy systems of electric power, district heating, and natural gas, providing a valuable foundation for the study of IES dynamic simulations. For EPSs, transient simulation methods mainly employ differential algebraic equations (DAEs) to describe the electrical and mechanical dynamics [10]. Variable-step algorithms have been proven effective in enhancing the simulation efficiency of multi-scale power systems, where the size of integration step can be adaptively adjusted according to the time constant [11]. DHSs are usually modeled using partial differential equations (PDEs). Numerical methods, such as the implicit upwind method, are commonly adopted to solve the DHS models [12]. PDEs are also used to describe the dynamics of compressible gas flows in natural gas systems (NGSs), where the method of characteristics and the centered implicit difference algorithm have been successfully applied as solvers [13]. The intensive

interactions between the EPS and DHS make it possible to improve the economic and environmental performance of the IES, while posing new challenges and requirements on the simulation methods.

Although these methods have provided a foundation, there remain challenges to the simulation of IESs. The first concerns the heterogeneous characteristics resulting from the integration and coupling of multiple energy carriers. The time constants of the dynamics of electricity, heating, and natural gas vary from milliseconds to hours [14]. It is difficult for using a single algorithm to cover a wide range of time-scales while balancing the accuracy and speed. Moreover, the mathematical definitions and properties of the components of these systems are also quite different [15], which may present distinctive requirements for the solving algorithms. A unified framework that is compatible with different models and algorithms is required for the integration of multi-scale and multi-disciplinary energy dynamics in IESs.

A popular technique used to address the heterogeneous properties of an IES is the decoupling simulation method. For example, a two-time-scale method was developed in [16] for hybrid natural gas and electricity systems, where the dynamics of an EPS, NGS, and microturbines were considered. In [17], a model considering the dynamics of natural gas, electric power, and thermal energy was established and solved using a three-time-scale method based on the singular perturbation theory. In [15], an individual-based model was applied to analyze the heterogeneous dynamics of an IES under conditions of disturbances and faults, where the IES was divided into several individuals that interact with each other at fixed time intervals. In [18], an agent-based modeling method was developed for microgrids to realize the coupled dynamic behaviors of generators, energy storage devices and communication infrastructures. An event-driven co-simulation framework for interconnected power systems and communication networks was proposed in [19], which enabled the precise simulation of interactions among different components

such as power systems and communication networks.

The second challenge concerns the emerging hybrid continuous-discrete property within IESs. Many new technologies, such as smart control agents [20] and decentralized edge computing devices [21], are being used in IESs to exploit their intelligence properties. Compared with physical energy flows, cyber infrastructure, such as local temperature controllers, generally follows a completely different discrete behavior pattern. The discrete actions of numerous controllers consequently affect the dynamics of energy flows. In this case, the IES should be modeled as a hybrid system considering the cyber-physical interactions, in which discrete control events are triggered when specific energy states accumulate to a certain extent [22]. However, most conventional simulation algorithms are based on time discretization, which means that the frequent detection and location of discrete events significantly decrease the simulation efficiency [23]. Therefore, conventional methods cannot adequately address the simulation of an IES with hybrid continuous-discrete properties.

From a mathematical point of view, the simulation of hybrid continuous-discrete systems such as IESs can be defined as a series of initial value problems separated by events that lead to discrete changes. These events can be divided into time and state events. The exact occurrence time of a time event is scheduled in advance, while that of a state event is implicit because its occurrence is determined by the specific system states and thus more difficult to handle [24]. Quantized state system (QSS) simulation methods provide an effective way to simulate systems dominated by discrete features. State events can be precisely detected and processed with less computational effort compared with classic time-discretized integration methods. The basic idea can be illustrated using the first-order QSS (QSS1) method, which replaces the conventional time-discretization with the quantization of state variables [25]. Furthermore, high-order QSS methods have been investigated in [26] to enhance the accuracy and efficiency, while demonstrating

their feasibility in real applications such as simulations of phase-locked loop circuits [27] and power electronic systems [28]. Therefore, QSS methods can be considered as an alternative to time-discretized methods for the effective simulation of an IES with hybrid properties.

Despite the research efforts placed on the decoupling methods to solve IESs with heterogeneous characteristics resulting from the integration of multiple energy carriers, few studies have been oriented on the hybrid continuous-discrete properties brought by cyber devices. Although QSS methods have been used to solve the systems dominated by discrete properties, their applicability and adaptability have not been fully investigated in the IESs. A vital research gap exists in the methods to effectively simulate IESs with heterogeneous characteristics and hybrid continuous-discrete properties.

This paper proposes a simulation method for an electricity-heat integrated energy system (EH-IES) with hybrid continuous-discrete properties. The third-order QSS (QSS3) method is modified to solve a DHS with local temperature controllers, and subsequently applied for the co-simulation of an EH-IES under an event-driven framework. The study of this paper provides an efficient simulation method for highly-coupled EH-IES and can be used as an effective tool for the operation analysis, strategy verification, flexibility evaluation, etc. The main contributions are summarized as follows:

1) The modified QSS3 (MQSS3) method is developed for the simulation of a DHS with numerous local controllers. Compared with the conventional QSS3, MQSS3 combines QSS and time-discretized integration, and adopts an event detection and location mechanism to manage the numerous discrete controller actions. A higher efficiency is achieved with the proposed method in the simulation of DHS.

2) An event-driven framework is established to integrate MQSS3 in the EH-IES simulation. The

two subsystems, namely the EPS and DHS, are respectively solved using MQSS3 and time-discretized algorithms, and interact with each other through an event-driven interface. This framework enables the adoption of the most suitable models and algorithms for different systems to accommodate the heterogeneous properties.

3) Dynamic simulations of an EH-IES are performed using the proposed simulation method to demonstrate its advantages in efficiency. The results also prove that the proposed method accurately reveals the interactions between the thermal and electric dynamics, and can be utilized as an effective tool to analyze the potential of flexible cooperation of EPS and DHS.

The remainder of this paper is organized as follows. Section 2 presents the detailed modeling method for an EH-IES with hybrid continuous-discrete dynamics. Section 3 presents the methodology of MQSS3. Section 4 presents an event-driven simulation framework that integrates MQSS3 with conventional algorithms. Case studies are presented in Section 5 to verify the effectiveness of the proposed method. The discussion and conclusion are presented in Section 6.

2. Modeling of an EH-IES with hybrid continuous-discrete dynamics

2.1. Configuration of the EH-IES

Figure 1 shows a conceptual diagram of an EH-IES with power distribution networks, heat networks, electric heat sources, indoor fan coil units, and local controllers. It should be noted that there may be hundreds of buildings in a similar type as the heat loads. The power distribution network delivers electricity from the external power grid and distributed generators (DGs) to the electric loads. Electric boilers (EBs), which act as impacting electric loads, are used to supply thermal energy to buildings via the DHS pipelines for room heating. At the source and consumer side, many local temperature controllers participate in heat management to improve user experience. For example, the controller of the EB monitors the outlet temperature of the

heat transfer fluid (HTF) and controls the heating state of the EBs. The controller of the building monitors and adjusts the indoor temperature by switching on or off the fan coil unit. The interactions between the two networks through coupling components can provide flexibility to smooth the fluctuations in the power distribution network, which are brought by the uncertainties of electric power output from renewable DGs such as photovoltaic (PV) units and wind turbines.

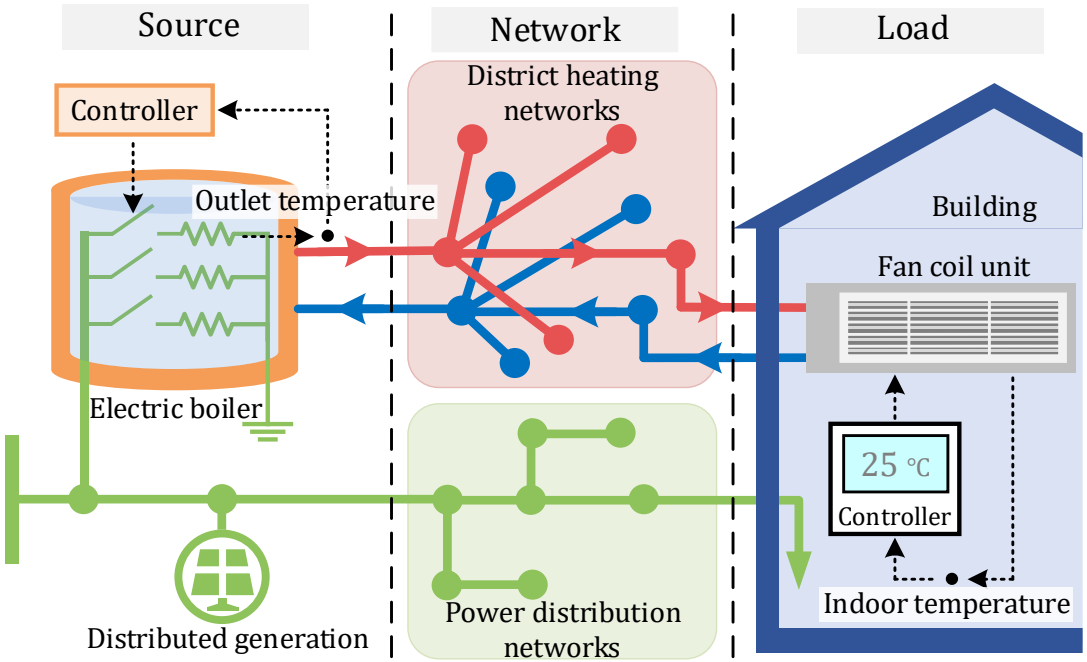

Fig. 1. Conceptual diagram of an EH-IES.

Detailed dynamic models of EPS and DHS should be constructed to consider the power fluctuations from PV units in the EPS, as well as the thermal energy storage potential from the pipelines and buildings in the DHS. The thermal storage potential is considered as virtual energy storage in the operation of EPS [29]. In this study, the simulation models include the DGs with controllers, electricity-heat coupling components, thermal inertia of networks, user-side buildings, and local temperature controllers. The functions of local temperature controllers in the DHS are to maintain temperature within certain range as well as enhance flexibility of the EPS. Commands from the controllers are determined by the system states such as flow rate and indoor

temperature, and in return affect the variation of the states in both the DHS and EPS. Hence, the discrete behaviors of the controllers are highly coupled with the energy flows of the EH-IES, making the dynamic models of the entire system sophisticated to be solved by classic integration algorithms.

2.2. Hybrid modeling methodology of the EH-IES

In this section, the hybrid continuous-discrete model of EH-IES is established and the coupling variables between the DHS and EPS are identified. The electricity-heat coupling dynamics are mainly described by conventional continuous models. The control systems are modeled based on simplified control strategies to describe the discrete properties of EH-IES.

2.2.1. Modeling of the heat networks

The dynamic model of pipelines is generally constructed using PDE, as shown in appendix A1. This PDE can be transformed into ordinary differential equations using the semi-discretized up-wind schemes [12] [30], as shown below:

$$\rho_{\mathrm{p}} c_{\mathrm{p}} A_{\alpha}^{\mathrm{p}} \frac{\mathrm{d}T_{\alpha,n}^{\mathrm{p}}}{\mathrm{d}t} + c_{\mathrm{p}} g_{\alpha}^{\mathrm{p}} \frac{T_{\alpha,n}^{\mathrm{p}} - T_{\alpha,n-1}^{\mathrm{p}}}{\Delta x} = \frac{1}{R_{\alpha}^{\mathrm{p}}} (T^{\mathrm{a}} - T_{\alpha,n}^{\mathrm{p}}) \tag{1}$$

where $T_{\alpha,n}^{\mathrm{p}}$ is the temperature of control volume n of the pipeline; $n = 1,2,\dots,N_{\alpha}$ denotes the number of control volume; N_{α} is the number of control volumes of pipeline α; Δx is the spatial step; ρ_{p} is the density of the HTF; c_{p} is the specific heat capacity of the HTF; A_{α}^{p} is the diameter of the pipeline and $A_{\alpha}^{\mathrm{p}} = \frac{\pi}{4}\left(D_{\alpha}^{\mathrm{p}}\right)^2$; D_{α}^{p} is the diameter of pipeline; R_{α}^{p} is the thermal resistance of the pipeline; T^{a} is the ambient temperature; g_{α}^{p} is the mass flow rate of the HTF flowing through pipeline α.

The heat network model can be obtained by combining (1) with the system topology. The boundary conditions are given by the flow continuity equations. The temperature of the HTF

leaving a node is calculated as the mixture temperature of the incoming flows [31]. Taking pipeline α as an example, its boundary condition is expressed as [32]:

$$T_{\alpha,0}^{\mathrm{p}} = T_{\alpha}^{\mathrm{n}} \tag{2}$$

where T_{α}^{n} is the temperature of the node connected to the inlet of pipeline α.

2.2.2. Modeling of the controllable EBs

The thermal response of the HTF in the EBs is taken for example to describe the thermal inertia characteristics [33], as shown in (3). As shown in (4), the heat power is influenced by the voltage fluctuations of the EPS as well as the number of active heating units.

$$c_{\mathrm{p}} m_{\beta}^{\mathrm{s}} \frac{\mathrm{d}T_{\beta}^{\mathrm{s,out}}}{\mathrm{d}t} = Q_{\beta}^{\mathrm{s}} - c_{\mathrm{p}} g_{\beta}^{\mathrm{s}} \left(T_{\beta}^{\mathrm{s,out}} - T_{\beta}^{\mathrm{s,in}}\right) \tag{3}$$

$$Q_{\beta}^{\mathrm{s}} = \frac{N_{\beta}^{\mathrm{s}} (U_{\beta}^{\mathrm{s}})^2}{R^{\mathrm{s}}} \tag{4}$$

where m_{β}^{s} is the mass of the HTF stored in EB β; $T_{\beta}^{\mathrm{s,in}}$ and $T_{\beta}^{\mathrm{s,out}}$ are the inlet and outlet temperatures of EB β, respectively; g_{β}^{s} is the mass flow rate of the HTF flowing through EB β; Q_{β}^{s} is the heat power; N_{β}^{s} is the number of active heating units; U_{β}^{s} is the voltage of the electricity node connected to EB β; R^{s} is the resistance of a heating unit; c_{p} is the specific heat capacity of the HTF.

The control objective of an EB is to ensure that the outlet temperature is maintained within a predefined range. The EBs are assumed to consist of a group of heating units, through which the heat power can be adjusted. A simple on/off control strategy is described by (5). The temperature is kept within the predefined interval by increasing or decreasing the number of active heating units when the outlet temperature reaches the lower or upper limits.

$$N_\beta^{\mathrm{s}} = \begin{cases} N_\beta^{\mathrm{s}} - 1\,,\ T_\beta^{\mathrm{s,out}} > T_\beta^{\mathrm{s,max}} \\ N_\beta^{\mathrm{s}} + 1\,,\ T_\beta^{\mathrm{s,out}} < T_\beta^{\mathrm{s,min}} \\ N_\beta^{\mathrm{s}}\ ,\ else \end{cases} \tag{5}$$

where $T_\beta^{\mathrm{s,max}}$ and $T_\beta^{\mathrm{s,min}}$ are the upper and lower limits of the outlet temperature, respectively.

2.2.3. Modeling of the heat loads with controllers

The heat load is modeled as a process in which a controllable fan coil unit dissipates heat to the indoor environment of a building with thermal inertia. An equivalent thermal model is adopted to establish the relations of the supply and return temperatures of the heat load, as shown below [33]:

$$c_{\mathrm{p}} m_\gamma^{\mathrm{f}} \frac{\mathrm{d}T_\gamma^{\mathrm{f,out}}}{\mathrm{d}t} = c_{\mathrm{p}} g_\gamma^{\mathrm{f}} \left(T_\gamma^{\mathrm{f,in}} - T_\gamma^{\mathrm{f,out}}\right) - S_\gamma^{\mathrm{f}} Q_\gamma^{\mathrm{f}} \tag{6}$$

$$Q_\gamma^{\mathrm{f}} = K_\gamma^{\mathrm{f}} A_\gamma^{\mathrm{f}} \left(\frac{T_\gamma^{\mathrm{f,in}} + T_\gamma^{\mathrm{f,out}}}{2} - T_\gamma^{\mathrm{b}}\right) \tag{7}$$

where m_γ^{f} is the mass of the HTF stored in fan coil unit γ installed in building γ; $T_\gamma^{\mathrm{f,in}}$ and $T_\gamma^{\mathrm{f,out}}$ are supply and return temperatures of fan coil unit γ, respectively; Q_γ^{f} is heat power produced by fan coil unit γ; S_γ^{f} is a Bool variable indicating the switch status; K_γ^{f} is heat transfer coefficient of the fan coil unit; A_γ^{f} is radiating area of the fan coil unit; g_γ^{f} is the mass flow rate of the HTF flowing through fan coil unit γ; T_γ^{b} is indoor temperature of building γ; c_{p} is the specific heat capacity of the HTF.

An isothermal air volume with a specific heat capacity is used to model the heated zones in each building. A first-order thermal model is adopted to describe the dynamic thermal process of an indoor environment, which can be expressed as follows:

$$\rho_{\mathrm{a}} c_{\mathrm{a}} V_\gamma^{\mathrm{b}} \frac{dT_\gamma^{\mathrm{b}}}{dt} = S_\gamma^{\mathrm{f}} Q_\gamma^{\mathrm{f}} - K_\gamma^{\mathrm{b}} V_\gamma^{\mathrm{b}} \left(T_\gamma^{\mathrm{b}} - T^{\mathrm{a}}\right) \tag{8}$$

where ρ_{a} is the density of indoor air; c_{a} is the specific heat capacity of indoor air; K_γ^{b} and V_γ^{b} are

volumetric heat index and peripheral volume of building γ, respectively.

The fan coil unit consists of a fan and a coil. The function of the fan is bringing heat from the coil into building and the coil is a closed pipe connecting the heating supply and return networks. The local temperature controller of the building is responsible for maintaining the indoor temperature within the comfortable range by switching on/off the fan coil unit in the room. The control logic is defined as follows:

$$S_\gamma^{\mathrm{f}} = \begin{cases} 0\ ,\ T_\gamma^{\mathrm{b}} > T_\gamma^{\mathrm{b,max}} \\ 1\ ,\ T_\gamma^{\mathrm{b}} < T_\gamma^{\mathrm{b,min}} \\ S_\gamma^{\mathrm{f}}\ ,\ else \end{cases} \tag{9}$$

where $T_\gamma^{\mathrm{b,max}}$ and $T_\gamma^{\mathrm{b,min}}$ are the upper and lower limits of the indoor temperature, respectively. This simplified on/off control strategy is taken as an example to represent the discrete properties in the system [34]. Other control strategies that are more complicated can be handled in simulations in a similar way.

2.2.4. Modeling of the power distribution networks

Several properties should be considered when modeling the power distribution networks, including the volt-ampere relations, network topologies, mechanical and control processes of the DGs, and power fluctuations. Based on the detailed models reported in [10], a compact expression for the electric power distribution network model in an EH-IES can be written as follows:

$$\begin{cases} \dot{\boldsymbol{x}}_{\mathrm{e}} = \boldsymbol{f}_{\mathrm{e}}(\boldsymbol{x}_{\mathrm{e}}, \boldsymbol{y}_{\mathrm{e}}) \\ \mathbf{0} = \boldsymbol{g}_{\mathrm{e}}(\boldsymbol{x}_{\mathrm{e}}, \boldsymbol{y}_{\mathrm{e}}, \boldsymbol{u}_{\mathrm{d}}^{\mathrm{c}}) \end{cases} \tag{10}$$

where $\boldsymbol{f}_{\mathrm{e}}$ and $\boldsymbol{g}_{\mathrm{e}}$ represent the differential and algebraic constraints in the network, respectively; The differential variables $\boldsymbol{x}_{\mathrm{e}}$ describe the dynamic process of various devices in distribution systems, such as the controller of distributed generators, the mechanical transient of rotating machines, etc. The algebraic equations mainly describe the constraints of distribution networks, which can be written as:

$$\boldsymbol{YU} = \boldsymbol{I} \tag{11}$$

where $\boldsymbol{Y}$ represents the admittance matrix of power distribution network determined by line parameters and electric loads; $\boldsymbol{U}$ represents the bus voltages in the network; $\boldsymbol{I}$ represents the injection currents in the network. The relations among the algebraic variables of the EPS, such as the bus voltages and electric loads, are also included in the algebraic equations of (10). $\boldsymbol{u}_{\mathrm{d}}^{\mathrm{c}}$ represents the vector of coupling variables between the DHS and EPS, i.e., electric loads of EBs connected to the power distribution network.

2.3. Holistic model description of an EH-IES

Equations (1) – (10) capture both the continuous and discrete dynamics of an EH-IES, which can be combined to formulate the entire model of the EH-IES according to the topological constraints, as shown in Fig. 2.

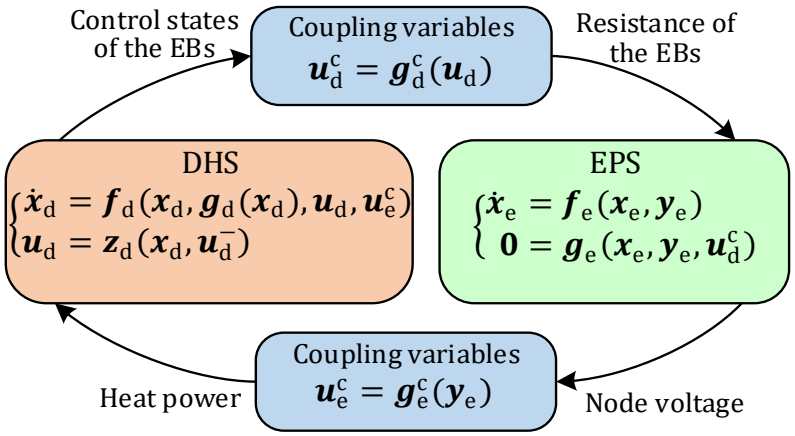

Fig. 2. Hybrid model description of an EH-IES.

As illustrated in Fig. 2, the models of the DHS and EPS are derived from Section 2.2. $\boldsymbol{f}_{\mathrm{d}}$ represents the differential equations containing the loads, sources, and networks of the DHS. $\boldsymbol{g}_{\mathrm{d}}$ represents the flow continuity equations describing the topology constraint of the DHS. The continuous state variables and discrete variables of the controllers are denoted by $\boldsymbol{x}_{\mathrm{d}}$ and $\boldsymbol{u}_{\mathrm{d}}$, respectively. $\boldsymbol{z}_{\mathrm{d}}$ represents the discrete logic of the controllers, indicating that the next control states

$\boldsymbol{u}_{\mathrm{d}}$ are dependent on the previous control states $\boldsymbol{u}_{\mathrm{d}}^{-}$. The DHS and EPS are coupled via $\boldsymbol{u}_{\mathrm{d}}^{\mathrm{c}}$ and $\boldsymbol{u}_{\mathrm{e}}^{\mathrm{c}}$, indicating that the electric voltage in the EPS affects the heating power of the EBs in the DHS, and in return, the control states of the EBs determine the load of the power distribution network.

3. QSS methods for the simulation of a DHS

3.1. Basic concept of the QSS method

In this section, the basic ideas of QSS methods are firstly analyzed to reveal their problems when applying in the simulation of EH-IES. QSS methods can be used as an alternative class of numerical integration methods to conventional time-discretized algorithms. In the QSS methods, a state variable does not change until its variation quantity exceeds a predefined unit, that is, the quantum. Considering the first-order ordinary differential equation group $\dot{\boldsymbol{x}} = \boldsymbol{f}(\boldsymbol{x}, t)$ as an example, the QSS replaces the state variables $\boldsymbol{x}$ by the quantized variables $\boldsymbol{q}$ to obtain the state-quantization model, as shown below:

$$\dot{\boldsymbol{x}} = \boldsymbol{f}(\boldsymbol{q}, t) \tag{12}$$

The value of $\boldsymbol{q}$ is determined by the quantization function, which is exclusively designed using different QSS algorithms. For example, QSS1 employs a quantization function, as shown below:

$$q_i(t) = \begin{cases} x_i(t), & |x_i(t) - q_i(t)| \geq \Delta Q \\ q_i\left(t_i^{\mathrm{L}}\right), & otherwise \end{cases} \tag{13}$$

where x_i and q_i are the ith elements of vectors $\boldsymbol{x}$ and $\boldsymbol{q}$; ΔQ is the quantum; t_i^{L} is the last update time of q_i. As defined in (13), q_i is updated when the difference between x_i and q_i reaches a quantum. Hence, with the QSS1 method, q_i follows a piecewise constant trajectory and x_i follows a piecewise linear trajectory [25]. The next update time of the quantized variables, denoted by t_i^{N} can be obtained from (14).

$$t_i^{\mathrm{N}} = \min\left\{t_i^{\mathrm{N}} \mid \left|x_i\left(t_i^{\mathrm{N}}\right) - q_i\left(t_i^{\mathrm{N}}\right)\right| = \Delta Q, t_i^{\mathrm{N}} > t\right\} \tag{14}$$

When applying QSS3 to a hybrid system consisting of numerous coupled continuous and discrete variables, as in the case of an EH-IES, the solving of (14) requires many repetitions and is thus time-consuming because each time a discrete change occurs, the next update time of numerous relevant variables must be recalculated. The detailed description of QSS3 method is shown in appendix A2.

3.2. Methodology of MQSS3

In this study, a MQSS3 method is proposed, in which the time discretization is combined with the state quantization of QSS3 to reduce the calculation effort for the next update time of the quantized variables.

1) Quantized integral formula

In MQSS3, in preparation for the next update step, the second-order and third-order derivatives of the state variables $\boldsymbol{x}_{\mathrm{d}}$ and quantized variables $\boldsymbol{q}_{\mathrm{d}}$ are defined and calculated as follows:

$$\begin{cases} \boldsymbol{x}_{\mathrm{d}}^{(1)}(t_{\mathrm{d}}) = \boldsymbol{f}_{\mathrm{d}}\left(\boldsymbol{q}_{\mathrm{d}}(t_{\mathrm{d}}), \boldsymbol{g}_{\mathrm{d}}\left(\boldsymbol{q}_{\mathrm{d}}(t_{\mathrm{d}})\right), \boldsymbol{u}_{\mathrm{d}}(t_{\mathrm{d}}), \boldsymbol{u}_{\mathrm{e}}^{\mathrm{c}}(t_{\mathrm{d}})\right) \\ \boldsymbol{x}_{\mathrm{d}}^{(2)}(t_{\mathrm{d}}) = \boldsymbol{f}_{\mathrm{d}}^{(1)}\left(\boldsymbol{q}_{\mathrm{d}}(t_{\mathrm{d}}), \boldsymbol{q}_{\mathrm{d}}^{(1)}(t_{\mathrm{d}}), \boldsymbol{u}_{\mathrm{d}}(t_{\mathrm{d}}), \boldsymbol{u}_{\mathrm{e}}^{\mathrm{c}}(t_{\mathrm{d}})\right) \\ \boldsymbol{x}_{\mathrm{d}}^{(3)}(t_{\mathrm{d}}) = \boldsymbol{f}_{\mathrm{d}}^{(2)}\left(\boldsymbol{q}_{\mathrm{d}}(t_{\mathrm{d}}), \boldsymbol{q}_{\mathrm{d}}^{(1)}(t_{\mathrm{d}}), \boldsymbol{q}_{\mathrm{d}}^{(2)}(t_{\mathrm{d}}), \boldsymbol{u}_{\mathrm{d}}(t_{\mathrm{d}}), \boldsymbol{u}_{\mathrm{e}}^{\mathrm{c}}(t_{\mathrm{d}})\right) \\ \boldsymbol{q}_{\mathrm{d}}(t_{\mathrm{d}}) = \boldsymbol{x}_{\mathrm{d}}(t_{\mathrm{d}}), \boldsymbol{q}_{\mathrm{d}}^{(1)}(t_{\mathrm{d}}) = \boldsymbol{x}_{\mathrm{d}}^{(1)}(t_{\mathrm{d}}), \boldsymbol{q}_{\mathrm{d}}^{(2)}(t_{\mathrm{d}}) = \boldsymbol{x}_{\mathrm{d}}^{(2)}(t_{\mathrm{d}}) \end{cases} \tag{15}$$

where t_{d} is the current update time of all the state and quantized variables; $\boldsymbol{x}_{\mathrm{d}}(t_{\mathrm{d}})$ is the result of the last update step; $\boldsymbol{q}_{\mathrm{d}}$ is the vector of quantized variables corresponding to $\boldsymbol{x}_{\mathrm{d}}$; $\boldsymbol{u}_{\mathrm{d}}$ and $\boldsymbol{u}_{\mathrm{e}}^{\mathrm{c}}$ are vectors of the non-differentiable discrete and algebraic variables.

To improve the simulation efficiency, a unified step size of the update time, denoted by h_{d}, is employed for all the state variables and quantized variables in MQSS3. Thus, the integral formulas in vector form can be used to update $\boldsymbol{x}_{\mathrm{d}}$ and $\boldsymbol{q}_{\mathrm{d}}$ to $t_{\mathrm{d}} + h_{\mathrm{d}}$, as shown in (16) and (17). These integral formulas are derived from the expansion of Taylor series.

$$\boldsymbol{x}_{\mathrm{d}}(t_{\mathrm{d}} + h_{\mathrm{d}}) = \boldsymbol{x}_{\mathrm{d}}(t_{\mathrm{d}}) + h_{\mathrm{d}}\boldsymbol{x}_{\mathrm{d}}^{(1)}(t_{\mathrm{d}}) + \frac{{h_{\mathrm{d}}}^2}{2}\boldsymbol{x}_{\mathrm{d}}^{(2)}(t_{\mathrm{d}}) + \frac{{h_{\mathrm{d}}}^3}{6}\boldsymbol{x}_{\mathrm{d}}^{(3)}(t_{\mathrm{d}}) \tag{16}$$

$$\boldsymbol{q}_{\mathrm{d}}(t_{\mathrm{d}}+h_{\mathrm{d}})=\boldsymbol{q}_{\mathrm{d}}(t_{\mathrm{d}})+h_{\mathrm{d}}\boldsymbol{q}_{\mathrm{d}}^{(1)}(t_{\mathrm{d}})+\frac{{h_{\mathrm{d}}}^{2}}{2}\boldsymbol{q}_{\mathrm{d}}^{(2)}(t_{\mathrm{d}}) \tag{17}$$

The unified step size of the update time is obtained by calculating the minimal value under the constraint of the quantization function for all the state variables, which is expressed as follows:

$$h_{\mathrm{d}}=\min\left\{h_{\mathrm{d}}\,\middle|\,\left|x_{\mathrm{d},i}(t_{\mathrm{d}}+h_{\mathrm{d}})-q_{\mathrm{d},i}(t_{\mathrm{d}}+h_{\mathrm{d}})\right|=\Delta Q, i=1,2,\dots N_{\mathrm{q}}\right\} \tag{18}$$

Substituting (15), (16), and (17) into (18), the explicit expression of h_{d} is derived as follows:

$$h_{\mathrm{d}}=\sqrt[3]{\frac{6\Delta Q}{\left|x_{\mathrm{d,max}}^{(3)}(t_{\mathrm{d}})\right|}} \tag{19}$$

where $x_{\mathrm{d,max}}^{(3)}(t_{\mathrm{d}})$ is the element with the largest absolute value in vector $\boldsymbol{x}_{\mathrm{d}}^{(3)}(t_{\mathrm{d}})$.

Equation (19) permits the explicit calculation of h_{d}, which avoids the repeated solving of high-order polynomial equations.

2) Detection and location of state events

From (19), it can be concluded that the step size is calculated based on the variation of the state variables. However, there are state events whose occurrence times are also dependent on the state variables and may fall within the next time step. For example, in an EH-IES, control actions are triggered if the temperature exceeds the upper or lower limits. These events must be precisely detected and handled to avoid loss of accuracy.

In MQSS3, the detection of a state event is performed for all discrete variables after an update step. The two conditions for event detection are defined as follows:

$$\left(x_{\mathrm{d},i}(t_{\mathrm{d}})-L^{\max}\right)<0\ \&\ \left(x_{\mathrm{d},i}(t_{\mathrm{d}})+\sum_{m=1}^{3}\frac{{h_{\mathrm{d}}}^{m}}{m!}x_{\mathrm{d},i}^{(m)}(t_{\mathrm{d}})-L^{\max}\right)\geq 0,\ \ i\in\Omega_{\mathrm{c}} \tag{20}$$

$$\left(x_{\mathrm{d},i}(t_{\mathrm{d}})-L^{\min}\right)>0\ \&\ \left(x_{\mathrm{d},i}(t_{\mathrm{d}})+\sum_{m=1}^{3}\frac{{h_{\mathrm{d}}}^{m}}{m!}x_{\mathrm{d},i}^{(m)}(t_{\mathrm{d}})-L^{\min}\right)\leq 0,\ \ i\in\Omega_{\mathrm{c}} \tag{21}$$

where Ω_{c} is the set of controlled variables; $x_{\mathrm{d},i}(i\in\Omega_{\mathrm{c}})$ is the controlled state variable in the DHS; $L^{\max}$ and $L^{\min}$ are the upper and lower limits of the controlled variables, respectively.

It is apparent that when (20) or (21) is satisfied, the occurrence time of the state event is within $(t_{\mathrm{d}}\,,t_{\mathrm{d}}+h_{\mathrm{d}}]$. Then, we must solve the third-order polynomial formulas, as shown in (22)

or (23), to determine the exact occurrence time.

$$x_{\mathrm{d},i}(t_\mathrm{d}) + \sum_{m=1}^{3} \frac{(t_i^{\mathrm{state}} - t_\mathrm{d})^m}{m!} x_{\mathrm{d},i}^{(m)}(t_\mathrm{d}) = L^{\max},\ t_i^{\mathrm{state}} \in (t_\mathrm{d}\,, t_\mathrm{d} + h_\mathrm{d}] \tag{22}$$

$$x_{\mathrm{d},i}(t_\mathrm{d}) + \sum_{m=1}^{3} \frac{(t_i^{\mathrm{state}} - t_\mathrm{d})^m}{m!} x_{\mathrm{d},i}^{(m)}(t_\mathrm{d}) = L^{\min},\ t_i^{\mathrm{state}} \in (t_\mathrm{d}\,, t_\mathrm{d} + h_\mathrm{d}] \tag{23}$$

where t_i^{state} is the occurrence time of the state event of $x_{\mathrm{d},i}$.

If more than one state event is located, the first one that occurs is selected and processed. The step size h_d should be adjusted to $t_i^{\mathrm{state}} - t_\mathrm{d}$ to capture the state event. The overall MQSS3 process is illustrated in the flowchart shown in Fig. 3. The initial and end times of the simulation are denoted by t_0 and t_{end}, respectively.

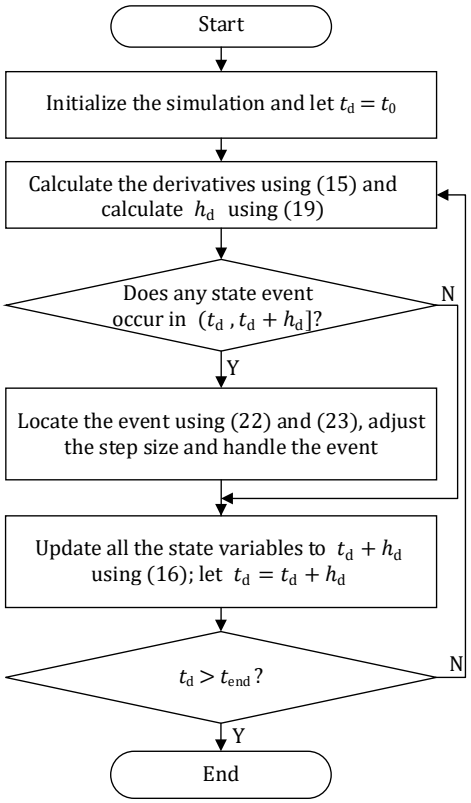

Fig. 3. Flowchart of the proposed MQSS3 algorithm.

3.3. Error analysis of MQSS3

1) Local truncation error analysis

To analyze the local truncation error of MQSS3, the Taylor expansion is applied to obtain the

exact solution at $t_\mathrm{d}+h_\mathrm{d}$, which is expressed as:

$$\widetilde{\boldsymbol{x}}_\mathrm{d}(t_\mathrm{d}+h_\mathrm{d})=\boldsymbol{x}_\mathrm{d}(t_\mathrm{d})+h_\mathrm{d}\boldsymbol{x}_\mathrm{d}^{(1)}(t_\mathrm{d})+\frac{{h_\mathrm{d}}^2}{2!}\boldsymbol{x}_\mathrm{d}^{(2)}(t_\mathrm{d})+\frac{{h_\mathrm{d}}^3}{3!}\boldsymbol{x}_\mathrm{d}^{(3)}(t_\mathrm{d})+\frac{{h_\mathrm{d}}^4}{4!}\boldsymbol{x}_\mathrm{d}^{(4)}(\xi)$$

$$\xi\in[t_\mathrm{d}\,,t_\mathrm{d}+h_\mathrm{d}] \tag{24}$$

where $\widetilde{\boldsymbol{x}}_\mathrm{d}(t_\mathrm{d}+h_\mathrm{d})$ is the exact solutions of the state variables at $t_\mathrm{d}+h_\mathrm{d}$; $\boldsymbol{x}_\mathrm{d}^{(i)}(t_\mathrm{d})$ is the ith-order derivatives of the state variables at t_d.

Compared with the numerical solution (16), the local truncation error $\boldsymbol{\varepsilon}_\mathrm{LTE}$ can be calculated as:

$$\boldsymbol{\varepsilon}_\mathrm{LTE}=\widetilde{\boldsymbol{x}}_\mathrm{d}(t_\mathrm{d}+h_\mathrm{d})-\boldsymbol{x}_\mathrm{d}(t_\mathrm{d}+h_\mathrm{d})=\frac{{h_\mathrm{d}}^4}{4!}\boldsymbol{x}_\mathrm{d}^{(4)}(\xi)=O\left({h_\mathrm{d}}^4\right) \tag{25}$$

From (25), it can be seen that the MQSS3 method has a third-order numerical accuracy. Substituting (19) into (25), the local truncation error can be calculated as:

$$\boldsymbol{\varepsilon}_\mathrm{LTE}=\frac{1}{4!}\left(\frac{6\Delta Q}{\left|x_{\mathrm{d,max}}^{(3)}(t_\mathrm{d})\right|}\right)^{\frac{4}{3}}\boldsymbol{x}_\mathrm{d}^{(4)}(\xi)\propto(\Delta Q)^{\frac{4}{3}} \tag{26}$$

From (26), it can be seen that the local truncation error can be controlled by the quantum ΔQ and is proportional to $(\Delta Q)^{\frac{4}{3}}$.

2) Global error analysis

With respect to the global error bound, it has been proved in [26] that for a linear time-invariant (LTI) system $\dot{\boldsymbol{x}}(t)=\boldsymbol{A}\boldsymbol{x}(t)+\boldsymbol{B}\boldsymbol{u}(t)$ solved using the QSS method, as long as (14) is satisfied, the global error $|\boldsymbol{e}(t)|$ is bounded by:

$$|\boldsymbol{e}(t)|\leq|\boldsymbol{V}||\mathbb{R}\mathrm{e}(\boldsymbol{\Lambda})^{-1}\boldsymbol{\Lambda}||\boldsymbol{V}^{-1}|\Delta Q \tag{27}$$

where $\boldsymbol{A}$ is a Hurwitz and diagonalizable matrix; $\boldsymbol{\Lambda}$ and $\boldsymbol{V}$ are the matrices of the eigenvalues and eigenvectors of $\boldsymbol{A}$, respectively ($\boldsymbol{\Lambda}$ is diagonal).

This conclusion can be easily extended to MQSS3 in an EH-IES. The integration process in MQSS3 can be divided into two parts. During ordinary integration of QSS3 without any state event, the next update time of all the state variables, $t_i^\mathrm{N},\ i=1,2,\dots N_\mathrm{q}$ can be obtained from (14).

In an update step of MQSS3, the next update time $t_\mathrm{d} + h_\mathrm{d}$ of all the state variables can be obtained from (18). When a state event occurs, the step size is further reduced, resulting in a stricter constraint than (27). By comparing (14) and (18), the relations of the next update times of QSS3 and MQSS3 are shown below:

$$t_i^{\mathrm{state}} \le t_\mathrm{d} + h_\mathrm{d} = \min\{\, t_i^{\mathrm{N}}, i = 1,2, \dots N_\mathrm{q} \,\} \tag{28}$$

With the same initial value of state variables, the step size of MQSS3 is smaller than that of QSS3. Therefore, the global error of MQSS3 is also bounded by (27) in the entire simulation. The analysis shows that the global error is bounded by a linear function of the quantum ΔQ.

4. Event-driven framework for the co-simulation of an EH-IES

MQSS3 provides an efficient solution approach for the DHS, in which numerous discrete behaviors of controllers are tightly coupled with continuous energy flows. In contrast, the EPS in our study is mainly composed of continuous states. The time constants of DG controllers and DG dynamics vary greatly, rendering the EPS more suitable for time-discretized variable-step algorithms. To combine MQSS3 with the time-discretized simulation method for EPSs, an event-driven framework was presented in this paper. Using the proposed event-driven framework, the EH-IES is modeled as a group of DAEs with discrete events, in which the subsystems are simulated individually according to the physical characteristics. When a discrete event occurs, all the affected subsystems must be reinitialized and the perturbation is transmitted from one subsystem to another in the form of events.

4.1. Definition of events

From an event-driven perspective, both the variation of continuous state variables and switching of discrete variables can be regarded as events. Each event has a timestamp indicating its occurrence time. Then, the occurrence times of all components are grouped and arranged in an

event-time table to drive the simulation process. Four types of events are defined in the proposed framework:

1) Event A: Internal update step in the DHS

Event A denotes an internal update step in the DHS that must be scheduled in advance in the event-time table. The timestamp of event A is $t_{\mathrm{d}} + h_{\mathrm{d}}$, where t_{d} is the current update time in the DHS, and h_{d} is the step size for the next internal update step. When event A is triggered, an internal update step should be performed in the DHS, which includes the following steps from (a1) to (a3):

(a1) Update all the state variables of the DHS to $t_{\mathrm{d}} + h_{\mathrm{d}}$ using (16) and let $t_{\mathrm{d}} = t_{\mathrm{d}} + h_{\mathrm{d}}$.

(a2) Calculate the timestamp for the next internal update step. Calculate the derivatives using (15) and calculate h_{d} using (19). Detect the state events using (20) and (21). If any state event occurs in $(t_{\mathrm{d}}, t_{\mathrm{d}} + h_{\mathrm{d}}]$, locate the state event based on (22) or (23), adjust the step size, and handle the event.

(a3) Update the coupling variables $\boldsymbol{u}_{\mathrm{d}}^{\mathrm{c}}$. The next internal update step in the DHS is added to the event-time table with the timestamp $t_{\mathrm{d}} + h_{\mathrm{d}}$. Detect the external event from the DHS to the EPS.

2) Event B: Internal update step in the EPS

Event B denotes an internal update step in the EPS that must be scheduled in advance in the event-time table. The timestamp of event B is $t_{\mathrm{e}} + h_{\mathrm{e}}$, where t_{e} is the current update time in the EPS, and h_{e} is the step size for the next internal update step. When event B is triggered, an internal update step should be performed in the EPS, which includes the following steps from (b1) to (b3):

(b1) Update all the state variables of the EPS to $t_{\mathrm{e}} + h_{\mathrm{e}}$ according to the EPS integration algorithm and let $t_{\mathrm{e}} = t_{\mathrm{e}} + h_{\mathrm{e}}$.

(b2) Calculate the timestamp of the next update step under the preset numerical precision according to the EPS integration algorithm.

(b3) Update the coupling variables $\boldsymbol{u}_{\mathrm{e}}^{\mathrm{c}}$. The next update step in the EPS is added to the event-time table with the timestamp $t_{\mathrm{e}} + h_{\mathrm{e}}$. Detect the external event from the EPS to the DHS.

3) Event C: External event from the DHS to the EPS

Event C demonstrates the impact of the DHS dynamics on the EPS, that is, the variation in the electric load due to the switching of the EBs. The triggering criterion for event C is defined as follows:

$$\left|u'_{\mathrm{d},k} - u''_{\mathrm{d},k}\right| > 0, k \in \Omega_{\mathrm{s}} \tag{29}$$

where $u'_{\mathrm{d},k}$ represents the current value of discrete variable k; $u''_{\mathrm{d},k}$ represents the value of discrete variable k when event B was last triggered; Ω_{s} denotes the set of control states of the EBs. When event C is triggered, the coupling variables $\boldsymbol{u}_{\mathrm{d}}^{\mathrm{c}}$ are updated, and the next update step in the EPS should be rescheduled.

4) Event D: External event from the EPS to the DHS

Event D demonstrates the impact of the EPS dynamics on the DHS, that is, the variation in the heating power of the EBs due to voltage fluctuations. The triggering criterion for event D is defined as follows:

$$\left|y'_{\mathrm{e},k} - y''_{\mathrm{e},k}\right| \geq \Delta y_{\mathrm{e}}\,, k \in \Omega_{\mathrm{v}} \tag{30}$$

where $y'_{\mathrm{e},k}$ represents the value of algebraic variable k at the current time; $y''_{\mathrm{e},k}$ represents the value of algebraic variable k when event A was last triggered; Ω_{v} represents the set of voltages of the electricity nodes connected to the EBs; Δy_{e} represents the impact threshold. When event D is triggered, the coupling variables $\boldsymbol{u}_{\mathrm{e}}^{\mathrm{c}}$ are updated, and the next update step in the DHS should be rescheduled.

4.2. Formulation and execution of the event-time table

With the above-described four types of events, an event-time table can be formulated and used to execute the simulation procedure, as shown in Fig. 4.

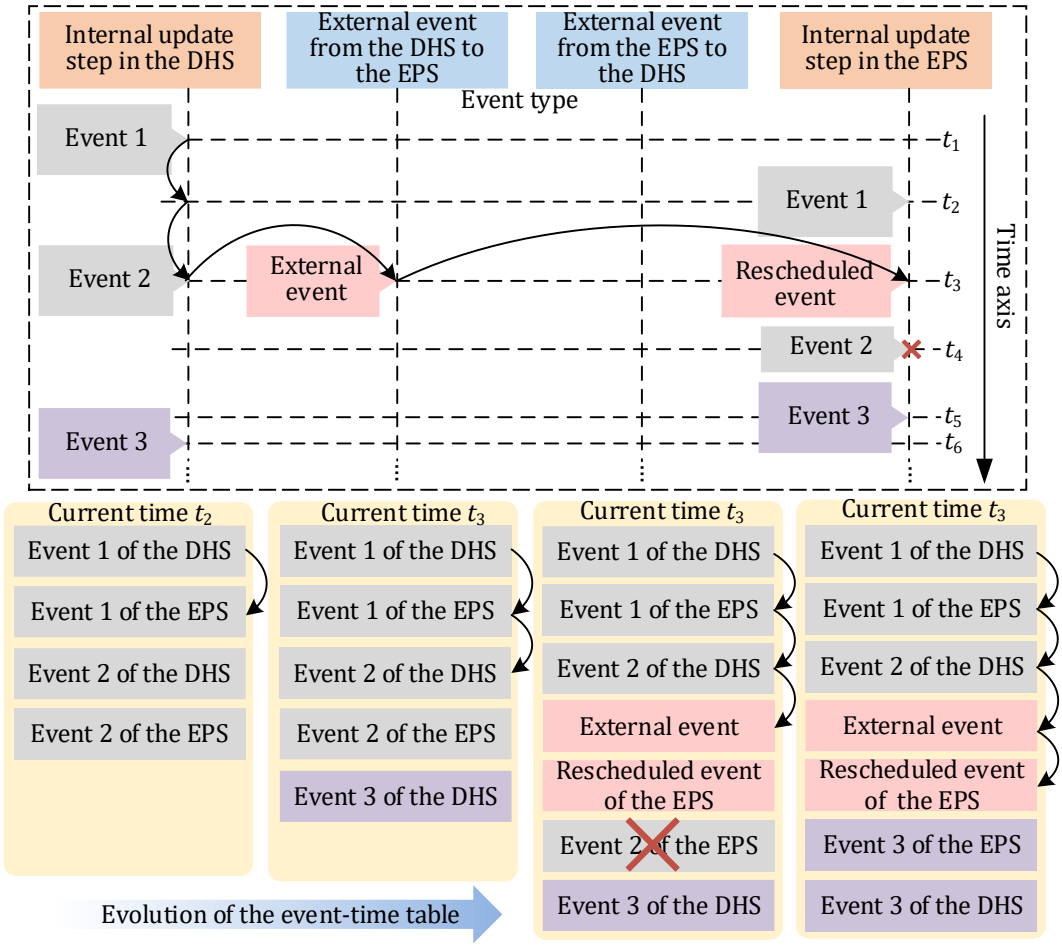

Fig. 4. Simulation process driven by the event-time table.

In Fig. 4, the internal events of the DHS and EPS are denoted by event n ($n = 1, 2, 3$). It is assumed that event 1 of the DHS and event 1 of the EPS have already been performed at t_2, and event 2 of the DHS and event 2 of the EPS have been added to the table and are waiting execution, as shown in the first block in Fig. 4. These internal events can be pre-scheduled because after each update step, the step size for the next update step can be calculated. As the simulation time advances, event 2 of the DHS is executed and event 3 of the DHS is added to the event-time table, as shown in the second block in Fig. 4.

The external events should be detected after each internal update step (i.e. internal events). As shown in the third block in Fig. 4, an external event from the DHS to the EPS is triggered following event 2 of the DHS. Then, the next internal update step of the EPS is rescheduled and replaces the original event 2 of the EPS. Finally, the rescheduled event of the EPS is executed and event 3 of the EPS is added to the table. The external event from the EPS to the DHS is manipulated in a similar manner.

By scheduling the event-time table, reasonable logic of the discrete actions and dependencies between different variables are guaranteed during the simulation. Thus, the event-driven framework provides an interactive interface for the co-simulation of the DHS and EPS using MQSS3 and conventional simulation methods.

The method presented above is illustrated in the flowchart shown in Fig. 5. The current and end times of the simulation are denoted by t and t_{end}, respectively.

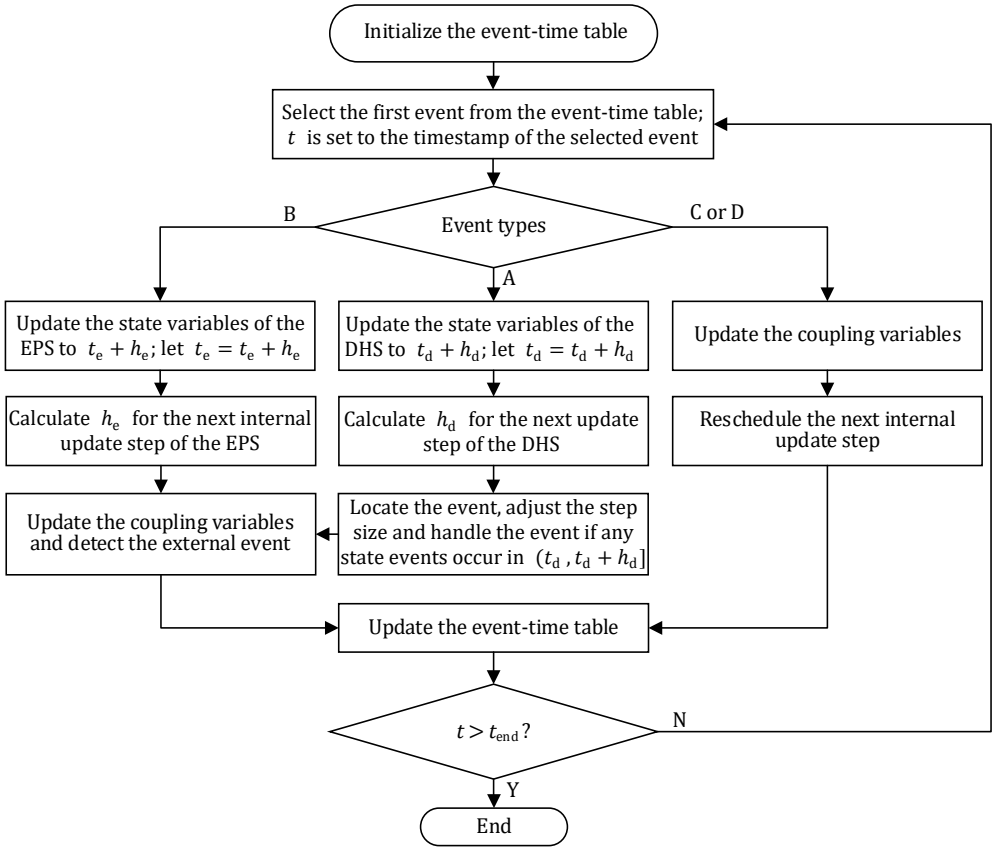

Fig. 5. Flowchart of the event-driven simulation framework.

5. Case studies

5.1. Structure of the studied case

The studied EH-IES consists of an EPS and a DHS as shown in Fig. 6. The EPS adopts the IEEE 33-node distribution network [35] with eight integrated PV units. The capacity of each PV system is 750 kW. The DHS contains a symmetrical heat supply and return network [31], three EBs as heat sources, and 21 heat load nodes. The heat energy is supplied to heat loads with heat loss along the pipelines and ten buildings for room heating at each node. The season is set as winter. The thermal parameters of the building and fan coil unit are presented in appendix B.

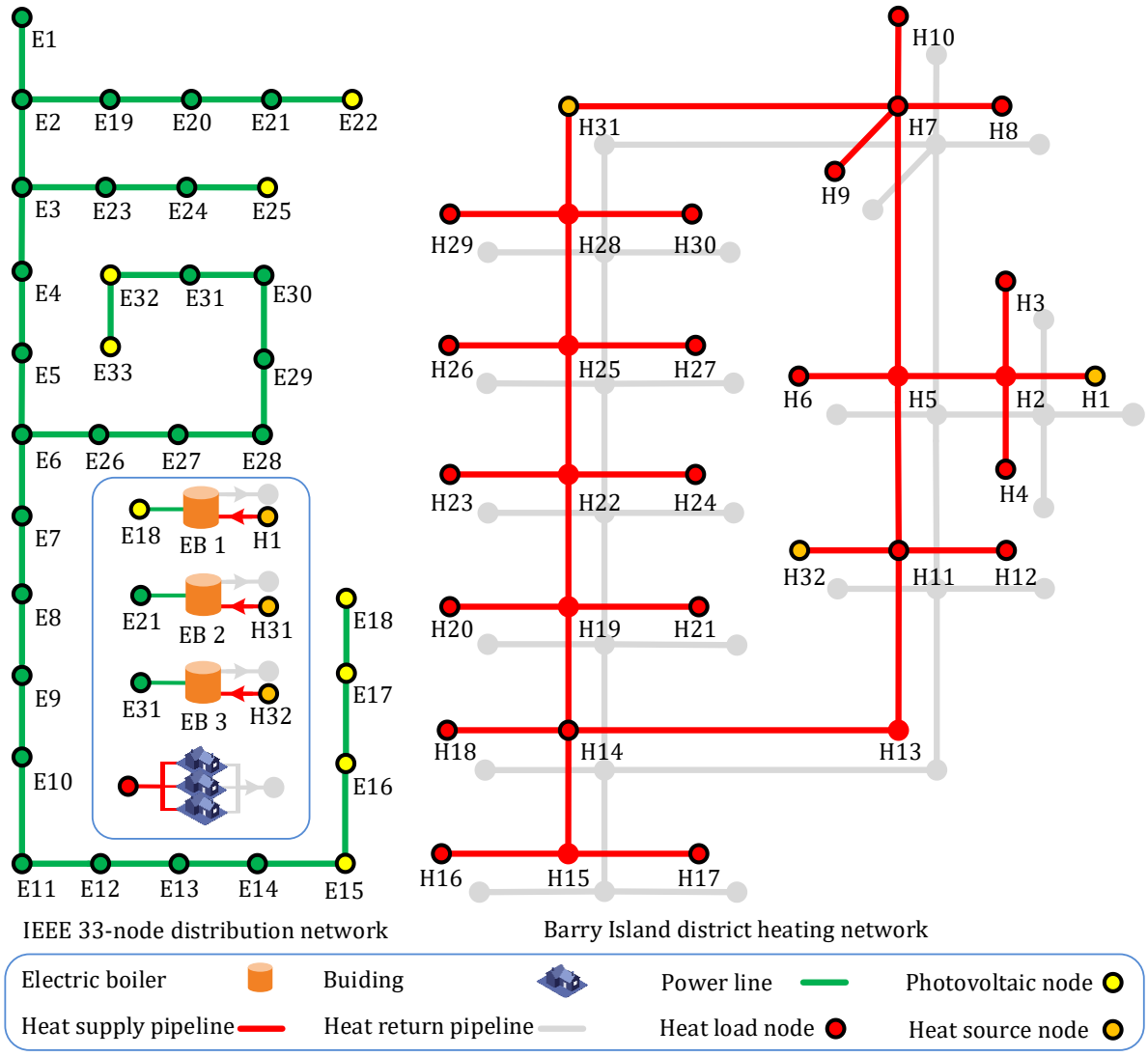

Fig. 6. System configuration of the studied EH-IES.

The rated power of each EB is 1 MW. Hence, the total PV capacity accounts for approximately 80% of the maximum electric load, forming a power distribution network with a high penetration of PV generation. The local temperature controllers in the DHS maintain the outlet temperature of the EBs in the range of 80 – 82 ℃. The indoor temperature of the buildings is maintained in the range of 24 – 25 ℃ by the local temperature controllers, introducing significant discrete properties into the simulation. A temperature sensor and controller are placed in each building. When the temperature reaches the upper limit or lower limit, the controller will be triggered to turn on/off the fan coil unit. To simplify the problem, the detailed factors are omitted such as the measuring error, the efficiency variation of devices, the hydraulic dynamics, and the protection devices. The district heating network adopts variable-temperature control strategy under constant flow rate [36]. The proposed simulation methods were implemented in MATLAB, and the simulations were conducted on a desktop computer with an Intel(R) Core (TM) i7-8700 CPU running at 3.20 GHz and 8 GB of RAM.

5.2. Performance comparison and analysis

Three methods were implemented to verify the efficiency of the proposed method, including:

1) Backward differentiation formula (BDF): The BDF in SUNDIALS, including a root-finding feature to locate state events [37], was employed to simultaneously solve the DHS and EPS. The relative tolerance was set to 1×10^{-8} and the absolute tolerance was set to 1×10^{-3} to obtain a benchmark of the simulation results.

2) QSS3-based method: The event-driven simulation that combines the conventional QSS3 with the BDF was employed to solve the DHS and EPS, respectively.

3) MQSS3-based method: The event-driven simulation that combines MQSS3 with the BDF was employed to solve the DHS and EPS, respectively.

The quantum values for QSS3 and MQSS3 were set to 1×10^{-5}. A 1-hour simulation was performed using the three methods described above. The ambient temperature, solar irradiance, and output power of a PV unit are shown in appendix B.

A comparison of the simulation results is presented in Fig. 7. The voltage of electricity node 21 is shown in Fig. 7(a). The voltage fluctuates rapidly with the output power of PV units. An instantaneous increase of voltage occurs at t_1 due to the disconnection of a heating unit. The outlet temperature of EB 2 is shown in Fig. 7(b). The outlet temperature reaches 82 ℃ at t_1. Then, the controller turns off a heating unit and the outlet temperature begins to go down gradually. The total power of EBs fluctuates with the voltage slightly, as shown in Fig. 7(c). At t_1, t_2, and t_3, the heating units are disconnected from the power grid resulting from the controller actions of EB 2, EB 1 and EB 3, which leads to the reduction of the total power from about 2.6 MW to 2 MW. In Fig. 7(d), the simulation result shows that with the actions of the local temperature controllers in the buildings, the indoor temperatures drawn with gray curves are maintained within the predefined interval.

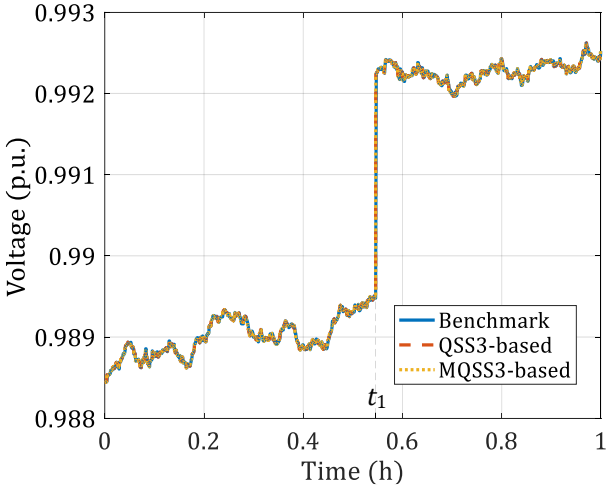

(a) Voltage of electricity node 21

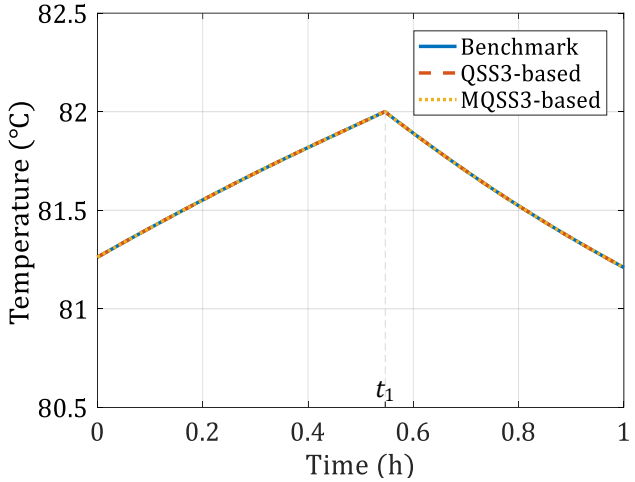

(b) Outlet temperature of EB 2

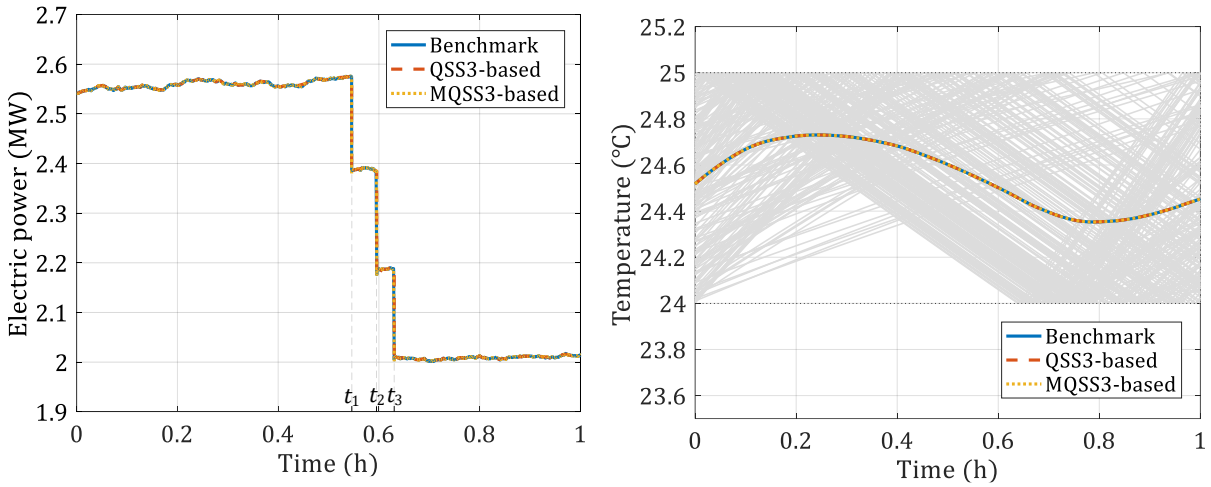

(c) Total electric power of the EBs (d) Average indoor temperature of the buildings

Fig. 7. Comparison of the simulation results.

The quantitative analysis of relative error is presented in Fig. 8. Both the QSS3-based and MQSS3-based methods exhibit adequate accuracy for the analysis of the EH-IES with the maximum error of 1.9×10^{-4} % and 1.2×10^{-5} %.

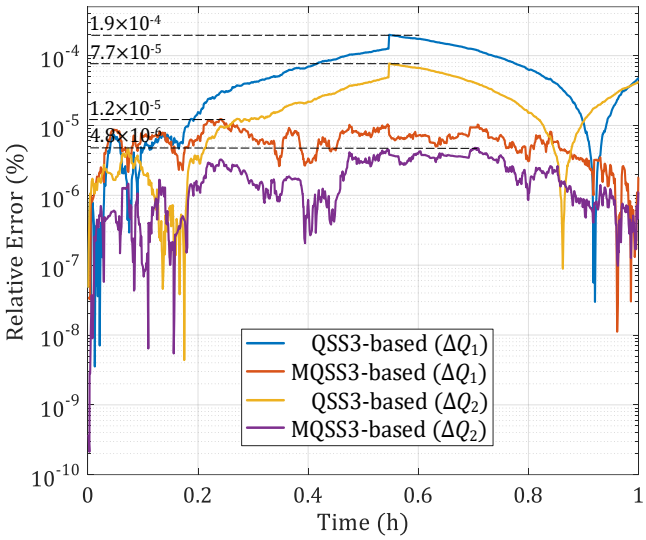

Fig. 8. Comparison between the errors of the QSS3-based and MQSS3-based methods.

Moreover, to explore the influence of the quantum on the simulation accuracy, different quantum values are selected as $\Delta Q_1 = 1 \times 10^{-5}$ and $\Delta Q_2 = 1 \times 10^{-6}$. As shown in Fig. 8, the MQSS3-based method guarantees better performance in terms of the simulation accuracy. The maximum error of QSS3-based method is 1.9×10^{-4} % and 1.2×10^{-5} % with the quantum of ΔQ_1

and ΔQ_2. The maximum error of MQSS3-based method is 7.7×10^{-5} % and 4.8×10^{-6} % with the quantum of ΔQ_1 and ΔQ_2. The error bound of MQSS3-based method is smaller than that of QSS3-based method. This is because MQSS3-based method selects the unified minimum step size for all the state variables in each step, which is smaller than that of QSS3-based method calculated for each state variable separately.

The calculation performance for the three methods is summarized in Table I. The BDF requires the longest time because of its inability to manage numerous local temperature controllers efficiently, which is unacceptable in real applications. Under the same quantum, the MQSS3-based method consumes only half the time required by the QSS3-based method, indicating the improved simulation efficiency achieved by MQSS3.

Table. I. Comparison of the calculation performance.

Method	Time cost (s)	
	ΔQ_1	ΔQ_2
QSS3-based method	30.0	56.7
MQSS3-based method	14.2	20.4
BDF	>1 h	

5.3. Simulation of the flexible cooperation of EH-IES

A test case is used to demonstrate the feasibility of the proposed method in real applications. The MQSS3-based method was used to simulate a 5-hour system operation scenario, in which the thermal inertia of the DHS was used to consume the excess PV output power and relieve voltage violations. Two operation strategies were simulated, including:

Strategy I: The DHS and EPS are controlled individually.

Strategy II: The operation of the DHS and EPS are coordinated. The upper limit of the outlet temperature of EBs is adjustable between 82 ℃ and 96 ℃ to provide flexibility for the EPS.

The ambient temperature, solar irradiance and output power of a PV unit are shown in appendix B. The simulation results for the DHS and EPS are shown in Fig. 9. It can be observed that the voltage of electricity node 18 violates the upper limit owing to the high penetration of PV generation between 11:00 and 14:00 under the strategy I. Correspondingly, under the strategy II, the output power of the EBs is increased, and the voltages of the EPS are effectively decreased to the normal range.

The dynamics with the strategies I and II in the DHS is illustrated in Fig. 10. At 11:00, because of the continuous increase in the node voltage, more heating units are activated in EB 1 to consume the excess PV power, and the upper limit of the outlet temperature of EB 1 is relaxed to 96 ℃.

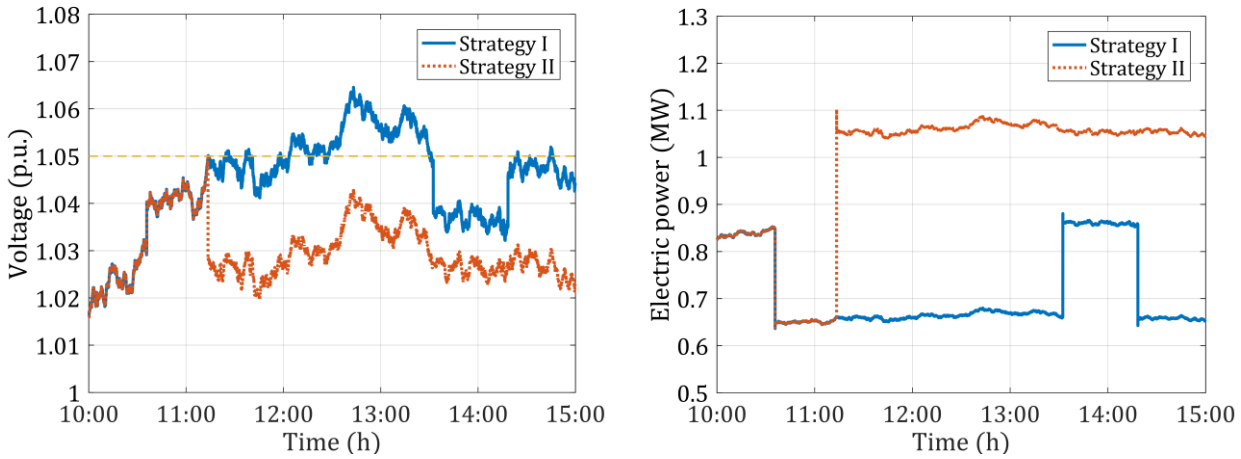

(a) Voltage of electricity node 18 (b) Electric power of EB 1

Fig. 9. Voltage of electricity node 18 and electric power of EB 1.

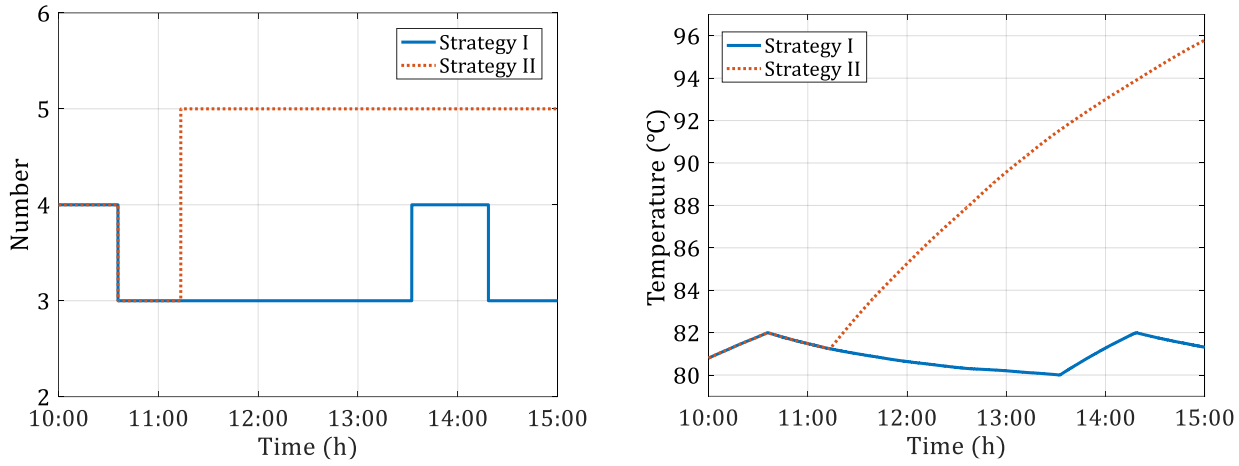

(a) Number of active heating units (b) Outlet temperature

Fig. 10. Control states and outlet temperature of EB 1.

The influence of the strategy II on the user-side is shown in Fig. 11. After the active response of EB 1 to voltage violation, the supply temperature of the user-side increases. However, under the constant temperature control of the local temperature controllers in the buildings, the heating time of the fan coil units is reduced, which guarantees that the consumers are not affected by the flexible response of the DHS.

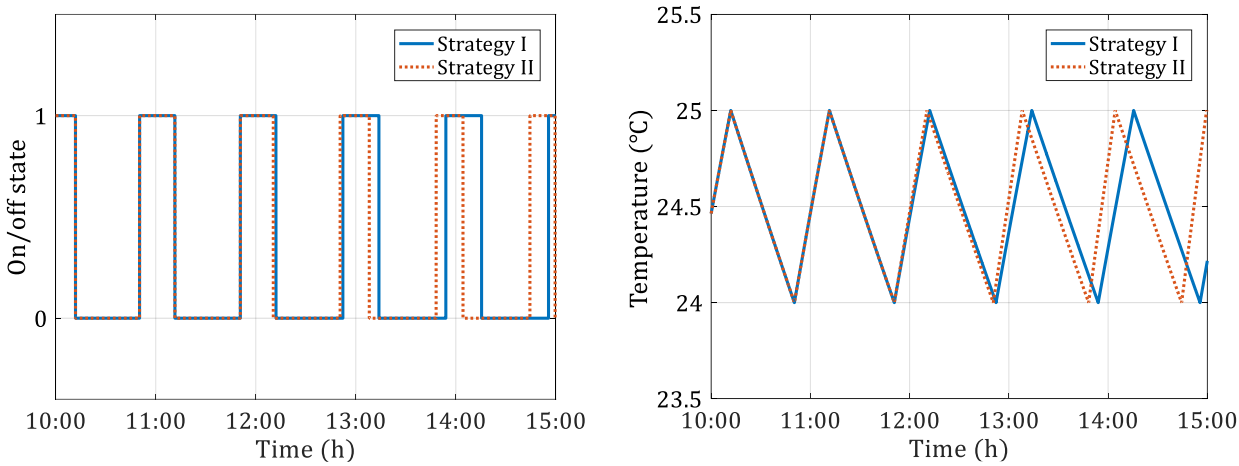

(a) On/off state of the fan coil unit (b) Indoor temperature

Fig. 11. Control states and indoor temperature of building 1.

A similar conclusion can be drawn from the average temperature of all the buildings (210

buildings in total), as shown in Fig. 12. It is demonstrated that with the actions of the local temperature controllers, the indoor temperature under both operation strategies is maintained within a predefined interval. Furthermore, the frequent actions of the controllers introduce numerous discrete changes into the simulation, indicating the ability of the proposed MQSS3-based method to effectively and efficiently simulate a continuous-discrete hybrid IES.

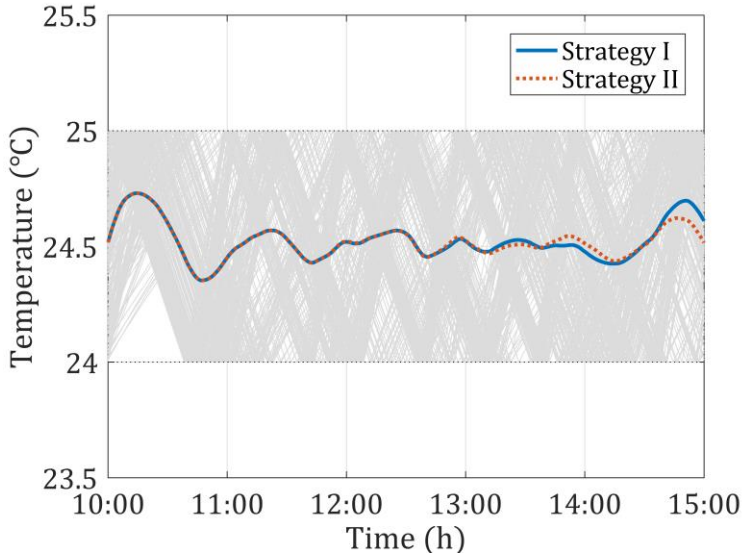

Fig. 12. Average indoor temperature of all buildings.

5.4. Simulation of the EH-IES with faults

A scenario is simulated to verify the effectiveness of the method under fault conditions. Three-phase short-circuit occurs at node 21 in the power distribution network. The fault is cleared after 0.2 s and then heating units of EB 2 are all disconnected from the power grid. After half an hour, power supply of EB 2 is restored by the operators. Other settings and inputs are the same as that of Section 5.3.

After the short circuit, all heating units of EB 2 are disconnected from the power grid, resulting in the decrease of outlet temperature. From the normal operation states before the fault, it can be derived that five heating units need to be activated if the outlet temperature is required to

reach 82 ℃. Therefore, five heating units of EB 2 are all restarted near 11:00 and the outlet temperature begins to increase, as shown in Fig. 13(a) and Fig. 13(b). Due to the short-circuit in the power grid, the voltage of node 21 drops instantaneously lasting for 0.2 s, as shown in Fig. 13(c). It can be seen from Fig. 13(d) that the heating time of the building becomes longer due to the falling of the outlet temperature of EB 2. The results show that the proposed method can reveal the system dynamics under fault conditions.

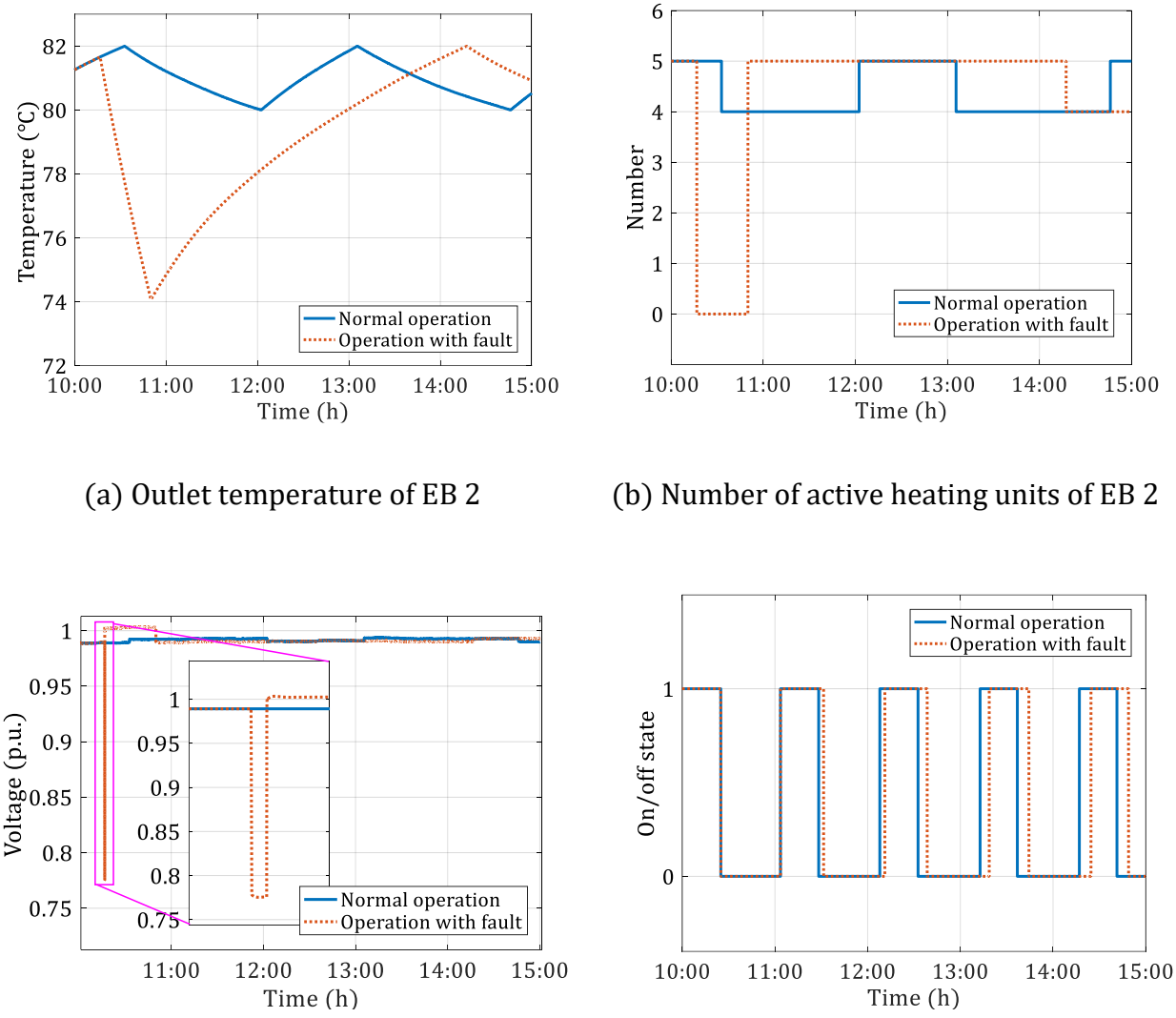

(a) Outlet temperature of EB 2

(b) Number of active heating units of EB 2

(c) Voltage of electricity node 21

(d) On/off state of the fan coil unit

Fig. 13. Comparison of the simulation results.

6. Conclusion

With the introduction of the digitalization and intellectualization trends in energy systems, the simulation of continuous-discrete hybrid systems considering both energy and cyber characteristics is becoming increasing essential for the development of IESs. In this paper, the MQSS3 method with third-order numerical accuracy and global error bound was proposed to address the simulation of energy systems, in which QSS and time-discretized integration were integrated to improve the simulation efficiency. The MQSS3 method was further integrated with the time-discretization based BDF under an event-driven framework, which improves the applicability of MQSS3 to accommodate the heterogeneous properties of IESs. A community-scale EH-IES with 210 buildings and maximum 80% PV penetration was used as an example to verify the proposed simulation methods under flexible cooperation and fault conditions. The results show that the efficiency of MQSS3-based method is improved by nearly onefold compared with the QSS3-based method under the same error level.

The study of this paper provides an efficient simulation method for highly-coupled EH-IES to reveal the interaction processes between DHS and EPS. It can be used as an effective tool for the operation analysis, strategy verification, flexibility evaluation, etc. With the real-time measurement of operation states, loads and external environment information, the simulation method can also be used as an online analysis tool for the optimal dispatch, risk identification, and preventive control of IESs.

In the future, the studies can be improved from the following aspects. Firstly, to highlight the simulation methodology, the physical dynamics as well as the control strategies of the EH-IES in this paper are simplified. Detailed and advanced models can be included, such as the efficiency of devices under various working conditions, hydraulic dynamics, and inertia of measurement, to establish a more realistic condition for simulation verification. Secondly, the simulation scale

is limited in a community or regional system in this paper. It can be further extended to larger scale such as a city via model aggregation or parallel computing of different subsystems, which is naturally enabled by the proposed event-driven framework. Thirdly, the selection of quantum value ΔQ is empirical in this study, which may further be optimized with a more accurate error estimation method or variable-order mechanism.

Acknowledgements

This work was supported by the National Natural Science Foundation of China (51961135101, 51907139) and Swedish Research Council (2018-06007).

Appendix A1

The heat networks are composed of nodes and pipelines. The dynamic model of pipelines describes the time delay and heat loss in the delivery process, which can be expressed by a PDE [12], as shown below:

$$\rho_{\mathrm{p}} c_{\mathrm{p}} A_{\alpha}^{\mathrm{p}} \frac{\partial T_{\alpha}^{\mathrm{p}}}{\partial t} + c_{\mathrm{p}} g_{\alpha}^{\mathrm{p}} \frac{\partial T_{\alpha}^{\mathrm{p}}}{\partial x} = \frac{1}{R_{\alpha}^{\mathrm{p}}} \left(T^{\mathrm{a}} - T_{\alpha}^{\mathrm{p}}\right) + \lambda \frac{d^2 T_{\alpha}^{\mathrm{p}}}{dx^2} \tag{A1}$$

where T_{α}^{p} is the temperature of the HTF in pipeline α; ρ_{p} is the density of the HTF; c_{p} is the specific heat capacity of the HTF; A_{α}^{p} is the diameter of the pipeline and $A_{\alpha}^{\mathrm{p}} = \frac{\pi}{4}\left(D_{\alpha}^{\mathrm{p}}\right)^2$; D_{α}^{p} is the diameter of pipeline; R_{α}^{p} is the thermal resistance of the pipeline; T^{a} is the ambient temperature; g_{α}^{p} is the mass flow rate of the HTF flowing through pipeline α; λ is the thermal conductivity of the HTF. The conduction term, $\lambda \frac{d^2 T_{\alpha}^{\mathrm{p}}}{dx^2}$ can be omitted to further simplify the equation [38]:

$$\rho_{\mathrm{p}} c_{\mathrm{p}} A_{\alpha}^{\mathrm{p}} \frac{\partial T_{\alpha}^{\mathrm{p}}}{\partial t} + c_{\mathrm{p}} g_{\alpha}^{\mathrm{p}} \frac{\partial T_{\alpha}^{\mathrm{p}}}{\partial x} = \frac{1}{R_{\alpha}^{\mathrm{p}}} \left(T^{\mathrm{a}} - T_{\alpha}^{\mathrm{p}}\right) \tag{A2}$$

Appendix A2

High-order QSS methods adopt more complicated quantization functions to improve the accuracy. For example, in QSS3, the value of q_i is determined by the second-order quantization function, as shown below:

$$q_i(t) = \begin{cases} x_i(t), & |x_i(t) - q_i(t)| \geq \Delta Q \\ q_i\left(t_i^{\mathrm{L}}\right) + \left(t - t_i^{\mathrm{L}}\right) q_i^{(1)}\left(t_i^{\mathrm{L}}\right) + \frac{\left(t - t_i^{\mathrm{L}}\right)^2}{2} q_i^{(2)}\left(t_i^{\mathrm{L}}\right), & otherwise \end{cases} \tag{A3}$$

Hence, with QSS3, $q_i(t)$ follows a piecewise quadratic trajectory and $x_i(t)$ follows a piecewise cubic trajectory. Assuming q_i as the latest updated variable at the current time t, the next update time of q_i, denoted by t_i^{N}, can be calculated by an explicit expression derived from (A4) [39].

$$t_i^{\mathrm{N}} = t + \sqrt[3]{\frac{6\Delta Q}{\left|x_i^{(3)}(t)\right|}} \tag{A4}$$

After the update of q_i, the next update time of q_j that is dependent on q_i must be recalculated

by solving an equation containing third-order polynomial items derived from (A5).

$$\left|x_j(t) - q_j(t) + e(x_j^{(1)}(t) - q_j^{(1)}(t)) + \frac{e^2}{2}(x_j^{(2)}(t) - q_j^{(2)}(t)) + \frac{e^3}{6}x_j^{(3)}(t)\right| = \Delta Q \qquad \text{(A5)}$$

where $e = t_j^{\mathrm{N}} - t$. The detailed procedure of QSS3 is presented as follows.

Procedure of the QSS3 algorithm

while $t < t_{\mathrm{end}}$ // simulate until the end time
  $t = \min(\boldsymbol{t}^{\mathrm{N}})$ // advance the simulation time
  $i = \mathrm{argmin}(\boldsymbol{t}^{\mathrm{N}})$ // quantized variable i is updated first
  $e = t - t_i^{\mathrm{L}}$ // elapsed time since the last update
  $x_i(t) = x_i(t_i^{\mathrm{L}}) + ex_i^{(1)}(t_i^{\mathrm{L}}) + \frac{e^2}{2}x_i^{(2)}(t_i^{\mathrm{L}}) + \frac{e^3}{6}x_i^{(3)}(t_i^{\mathrm{L}})$ // update state variable i
  $x_i^{(1)}(t) = x_i^{(1)}(t_i^{\mathrm{L}}) + ex_i^{(2)}(t_i^{\mathrm{L}}) + \frac{e^2}{2}x_i^{(3)}(t_i^{\mathrm{L}}), x_i^{(2)}(t) = x_i^{(2)}(t_i^{\mathrm{L}}) + ex_i^{(3)}(t_i^{\mathrm{L}})$
  // update the state variable i
  $x_i^{(1)}(t) = f_i(\boldsymbol{q}(t), t)$, $x_i^{(2)}(t) = f_i^{(1)}(\boldsymbol{q}(t), \boldsymbol{q}^{(1)}(t), t)$,
  $x_i^{(3)}(t) = f_i^{(2)}(\boldsymbol{q}(t), \boldsymbol{q}^{(1)}(t), \boldsymbol{q}^{(2)}(t), t)$
  // update the state derivatives
  // quantized variables are calculated by the quantization function
  $t_i^{\mathrm{N}} = \min(\tau > t)$ subject to $|x_i(\tau) - q_i(\tau)| = \Delta Q$ // calculate the next update time
  $t_i^{\mathrm{L}} = t$ // the last update time
  for each j that x_j depend on q_i (x_i is not included)
    $e = t - t_j^{\mathrm{L}}$ // elapsed time since the last update
    $x_j(t) = x_j(t_j^{\mathrm{L}}) + ex_j^{(1)}(t_j^{\mathrm{L}}) + \frac{e^2}{2}x_j^{(2)}(t_j^{\mathrm{L}}) + \frac{e^3}{6}x_j^{(3)}(t_j^{\mathrm{L}})$ // update the state variable
    $x_j^{(1)}(t) = f_j(\boldsymbol{q}(t), t)$, $x_j^{(2)}(t) = f_j^{(1)}(\boldsymbol{q}(t), \boldsymbol{q}^{(1)}(t), t)$,
    $x_j^{(3)}(t) = f_j^{(2)}(\boldsymbol{q}(t), \boldsymbol{q}^{(1)}(t), \boldsymbol{q}^{(2)}(t), t)$
    // update the state derivatives
    // quantized variables are calculated by the quantization function
    $t_j^{\mathrm{N}} = \min(\tau > t)$ subject to $\left|x_j(\tau) - q_j(\tau)\right| = \Delta Q$ // recalculate the next update time
    $t_j^{\mathrm{L}} = t$ // the last update time
  end for
end while

Appendix B

Table B.1 presents some thermal parameters of the building and fan coil unit. The ambient temperature and solar irradiance over 1 hour are shown in Fig. B.1. The ambient temperature and solar irradiance over 5 hours from 10:00 to 15:00 are shown in Fig. B.2. The output power of a PV unit over 1 hour is shown in Fig. B.3(a). The output power of a PV unit over 5 hours from 10:00 to 15:00 is shown in Fig. B.3(b).

Table. B1. Thermal parameters.

Parameter	Value	Parameter	Value
K_γ^{b}	2.3×10^{-2}	K_γ^{f}	8
V_γ^{b}	540	A_γ^{f}	2.5

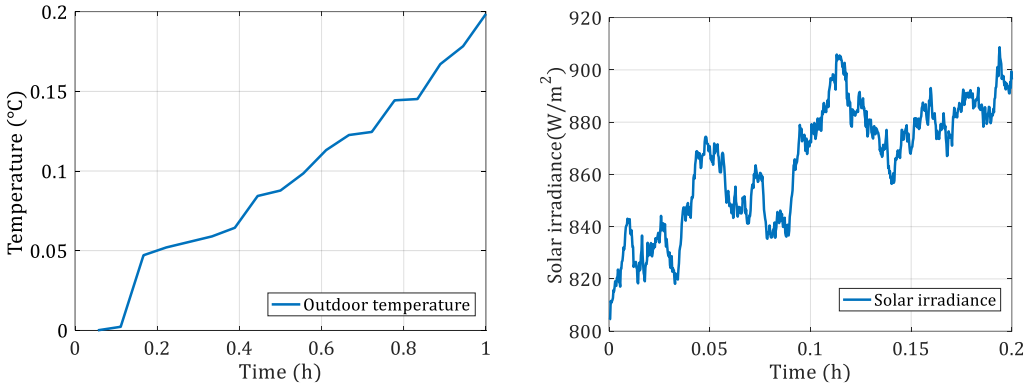

(a) Ambient temperature (b) Solar irradiance

Fig. B1. Ambient temperature and solar irradiance over 1 hour.

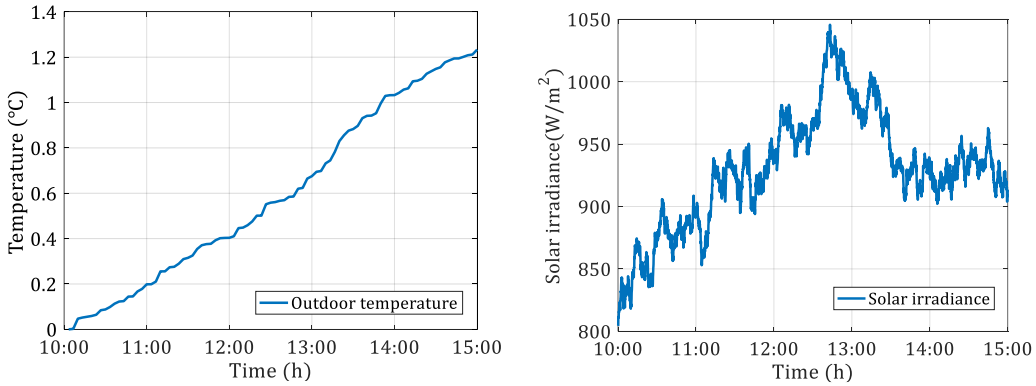

(a) Ambient temperature (b) Solar irradiance

Fig. B2. Ambient temperature and solar irradiance over 5 hours.

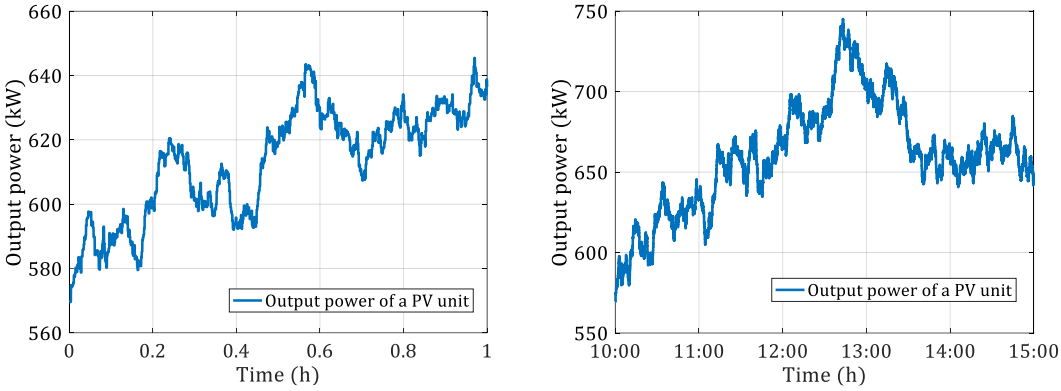

(a) Output power over 1 hour (b) Output power over 5 hours

Fig. B3. Output power of a PV unit.

References

[1] Perera A, Javanroodi K, Wang Y, et al. Urban cells: Extending the energy hub concept to facilitate sector and spatial coupling. Advances in Applied Energy 2021; 3: 100046. https://doi.org/10.1016/j.adapen.2021.100046.

[2] Anderson A, Suryanarayanan S. Review of energy management and planning of islanded microgrids. CSEE Journal of Power and Energy Systems 2020; 6(2): 329-343. https://doi.org/10.17775/CSEEJPES.2019.01080.

[3] Fan H, Yu Z, Xia S, et al. Review on coordinated planning of source-network-load-storage for integrated energy systems. Frontiers in Energy Research 2021; 9: 138. https://doi.org/10.3389/fenrg.2021.641158.

[4] Li C, Li P, Yu H, et al. Optimal planning of community integrated energy station considering frequency regulation service. Journal of Modern Power Systems and Clean Energy 2021; 9(2): 264-273. https://doi.org/10.35833/MPCE.2019.000056.

[5] Zhu M, Xu C, Dong S, et al. An integrated multi-energy flow calculation method for electricity-gas-thermal integrated energy systems. Protection and Control of Modern Power Systems 2021; 6(1): 5. https://doi.org/10.1186/s41601-021-00182-2.

[6] Mu Y, Meng X, Du L, et al. User-friendly rolling control strategy for a heat pump heating system considering building thermal inertia. IET Energy Systems Integration 2020; 2(4): 393-403. https://doi.org/10.1049/iet-esi.2020.0059.

[7] Marnay C, Asano H, Papathanassiou S, et al. Policymaking for microgrids. IEEE Power and Energy Magazine 2008; 6(3): 66-77. https://doi.org/10.1109/MPE.2008.918715.

[8] Nutkiewicz A, Choi B, Jain R. Exploring the influence of urban context on building energy retrofit performance: A hybrid simulation and data-driven approach. Advances in Applied Energy 2021; 3: 100038. https://doi.org/10.1016/j.adapen.2021.100038.

[9] Li H, Wang Z, Hong T, et al. Energy flexibility of residential buildings: A systematic review of characterization and quantification methods and applications. Advances in Applied Energy 2021; 3: 100054. https://doi.org/10.1016/j.adapen.2021.100054.

[10] Wang C, Yuan K, Li P, et al. A projective integration method for transient stability assessment of power systems with a high penetration of distributed generation. IEEE Transactions on Smart Grid 2018; 9(1): 386-395. https://doi.org/10.1109/TSG.2016.2553359.

[11] Astic J, Bihain A, Jerosolimski M. The mixed Adams-BDF variable step size algorithm to simulate transient and long term phenomena in power systems. IEEE Transactions on Power Systems 1994; 9(2): 929-935. https://doi.org/10.1109/59.317654.

[12] Wang Y, You S, Zhang H, et al. Thermal transient prediction of district heating pipeline: Optimal selection of the time and spatial steps for fast and accurate calculation. Applied Energy 2017; 206: 900-910. https://doi.org/10.1016/j.apenergy.2017.08.061.

[13] Yu S, Zhang S, Han Y, et al. Transfer function models of gas distribution networks for studying gas-electricity coupling: modeling, networking, and evaluation. International Journal of Electrical Power & Energy Systems 2020; 118: 105737. https://doi.org/10.1016/j.ijepes.2019.105737.

[14] Pan Z, Guo Q, Sun H. Interactions of district electricity and heating systems considering time-scale characteristics based on quasi-steady multi-energy flow. Applied Energy 2016; 167: 230-243. https://doi.org/10.1016/j.apenergy.2015.10.095.

[15] Wang L, Zheng J, Li M, et al. Multi-time scale dynamic analysis of integrated energy systems: An individual-based model. Applied Energy 2019; 237: 848-861. https://doi.org/10.1016/j.apenergy.2019.01.045.

[16] Xu X, Jia H, Chiang H, et al. Dynamic modeling and interaction of hybrid natural gas and electricity supply system in microgrid. IEEE Transactions on Power Systems 2015; 30(3): 1212-1221. https://doi.org/10.1109/TPWRS.2014.2343021.

[17] Shen F, Ju P, Shahidehpour M, et al. Singular perturbation for the dynamic modeling of integrated energy systems. IEEE Transactions on Power Systems 2020; 35(3): 1718-1728. https://doi.org/10.1109/TPWRS.2019.2953672.

[18] Kremers E, Gonzalez De Durana J, Barambones O. Multi-agent modeling for the simulation of a simple smart microgrid. Energy Conversion and Management 2013; 75: 643-650. https://doi.org/10.1016/j.enconman.2013.07.050.

[19] Lin H, Veda S, Shukla S, et al. GECO: Global event-driven co-simulation framework for interconnected power system and communication network. IEEE Transactions on Smart Grid 2012; 3(3): 1444-1456. https://doi.org/10.1109/TSG.2012.2191805.

[20] Zhang X, Manogaran G, Muthu B. IoT enabled integrated system for green energy into smart cities. Sustainable Energy Technologies and Assessments 2021; 46: 101208. https://doi.org/10.1016/j.seta.2021.101208.

[21] Feng C, Wang Y, Chen Q, et al. Smart grid encounters edge computing: opportunities and applications. Advances in Applied Energy 2021; 1: 100006. https://doi.org/10.1016/j.adapen.2020.100006.

[22] Palensky P, Widl E, Elsheikh A. Simulating cyber-physical energy systems: Challenges, tools and methods. IEEE Transactions on Systems, Man, and Cybernetics: Systems 2014; 44(3): 318-326. https://doi.org/10.1109/TSMCC.2013.2265739.

[23] Wetter M, Bonvini M, Thierry S. Nouidui. Equation-based languages - A new paradigm for building energy modeling, simulation and optimization. Energy and Buildings 2015; 117: 290-300. https://doi.org/10.1016/j.enbuild.2015.10.017.

[24] Park T, Barton P. State event location in differential-algebraic models. ACM Transactions on Modeling and Computer Simulation 1996; 6(2): 137-165. https://doi.org/10.1145/232807.232809.

[25] Kofman E, Junco S. Quantized-state systems: A DEVS approach for continuous system simulation. Simulation: Transactions of Society for Computer Simulation International 2001; 18(3): 123-132. https://doi.org/10.1177/003754970107700306.

[26] Kofman E. A third order discrete event simulation method for continuous system simulation. Latin American Applied Research 2006; 36(2): 101-108. https://doi.org/10.1007/0-387-30260-3.

[27] Jakobsson A, Serban A, Gong S. Implementation of quantized-state system models for a PLL loop filter using Verilog-AMS. IEEE Transactions on Circuits and Systems I: Regular Papers 2015; 62(3): 680-688. https://doi.org/10.1109/TCSI.2014.2377411.

[28] Li B, Zhao Z, Yang Y, et al. A novel simulation method for power electronics: discrete state event-driven method. CES Transactions on Electrical Machines and Systems 2017; 1(3): 273-282. https://doi.org/10.23919/TEMS.2017.8086106.

[29] Li Z, Wu W, Shahidehpour M, et al. Combined Heat and Power Dispatch Considering Pipeline Energy Storage of District Heating Network. IEEE Transactions on Sustainable Energy 2016; 7(1): 12-22. https://doi.org/10.1109/TSTE.2015.2467383.

[30] Ferziger JH, Peric M, Leonard A. Computational methods for fluid dynamics (4th edition). Berlin Heidelberg: Springer -Verlag; 2020. https://doi.org/10.1007/978-3-319-99693-6.

[31] Liu X, Wu J, Jenkins N, et al. Combined analysis of electricity and heat networks. Applied Energy 2016; 162: 1238-1250. https://doi.org/10.1016/j.apenergy.2015.01.102.

[32] Qin X, Sun H, Shen X, et al. A generalized quasi-dynamic model for electric-heat coupling integrated energy system with distributed energy resources. Applied Energy 2019; 251: 113270. https://doi.org/10.1016/j.apenergy.2019.05.073.

[33] Jiang X, Jing Z, Li Y, et al. Modelling and operation optimization of an integrated energy based direct district water-heating system. Energy 2014; 64: 375-388. https://doi.org/10.1016/j.energy.2013.10.067.

[34] Xu Y, Peet Y T. Effect of an on/off HVAC control on indoor temperature distribution and cycle variability in a single-floor residential building. Energy and Buildings 2021; 251: 111289. https://doi.org/10.1016/j.enbuild.2021.111289.

[35] Baran ME, Wu FF. Optimal capacitor placement on radial distribution systems. IEEE Transactions on Power Delivery 1989; 4(1): 725-734. https://doi.org/10.1109/61.19265.

[36] Zheng J, Zhou Z, Zhao J, et al. Effects of the operation regulation modes of district heating system on an integrated heat and power dispatch system for wind power integration. Applied Energy 2018; 230: 1126-1139. https://doi.org/10.1016/j.apenergy.2018.09.077.

[37] Hindmarsh A, Brown P, Grant K, et al. SUNDIALS: Suite of nonlinear and differential-algebraic equation solvers. ACM Transactions on Mathematical Software (TOMS) 2005; 31(3): 363-396. https://doi.org/10.1145/1089014.1089020.

[38] Duquette J, Rowe A, Wild P. Thermal performance of a steady state physical pipe model for simulating district heating grids with variable flow. Applied Energy 2016; 178: 383-393. https://doi.org/10.1016/j.apenergy.2016.06.092.

[39] Fernandez J, Kofman E. A stand-alone quantized state system solver for continuous system simulation. Simulation: Transactions of Society for Computer Simulation International 2014; 90(7): 782-799. https://doi.org/10.1177/0037549714536255.